1 # Patterns of mesozooplankton community composition and vertical fluxes in the global
2 # ocean

3

4 Yawouvi Dodji Soviadan[1], Fabio Benedetti[2], Manoela C. Brandão[1,3], Sakina-Dorothée
5 Ayata[1], Jean-Olivier Irisson[1], Jean Louis Jamet[5], Rainer Kiko[1], Fabien Lombard[1,4], Kissao
6 Gnandi[5], Lars Stemmann[1,*]
7
8 1 Sorbonne Université, CNRS, Laboratoire d'Océanographie de Villefranche, 06230
9 Villefranche-sur-mer, France.
10 2 Environmental Physics, Institute of Biogeochemistry and Pollutant Dynamics, ETH Zürich,
11 Universitätstrasse 16, 8092 Zürich, Switzerland.
12 3 Institut Français de Recherche pour l'Exploitation de la Mer, Centre Bretagne, 29280
13 Plouzané, France.
14 4 Institut Universitaire de France (IUF), Paris, France
15 5 Université de Toulon, Mediterranean Institute of Oceanology (MIO), AMU-UTLN UM110,
16 Equipe EMBIO. CS 60584, 83041 TOULON Cedex 9, FRANCE
17 6 Département de Géologie, Université de Lomé, Togo.
18 .
19
20 Corresponding author*
21
22

23 ## Abstract

24   Vertical variations in physical and chemical conditions drive changes in marine
25 zooplankton community diversity and composition. In turn, zooplankton communities play a
26 critical role in regulating the transfer of organic matter produced in the surface ocean to deeper
27 layers. Yet, the links between zooplankton community composition and the strength of vertical
28 fluxes of particles remain elusive, especially on a global scale. Here, we provide a
29 comprehensive analysis of variations in zooplankton community composition and vertical
30 particle flux in the upper kilometer of the global ocean. Zooplankton samples were collected
31 across five depth layers and vertical particle fluxes were assessed using continuous profiles of
32 the Underwater Vision Profiler (UVP5) at 57 stations covering seven ocean basins.
33 Zooplankton samples were analysed using a Zooscan and individual organisms were classified
34 into 19 groups for the quantitative analyses. Zooplankton abundance, biomass and vertical
35 particle flux decreased from the surface to 1000m depth at all latitudes. The zooplankton
36 abundance decrease rate was stronger at sites characterised by oxygen minima ($< 5\mu$mol O_2.kg^{-}
37 ^{1}) where most zooplankton groups showed a marked decline in abundance, except the
38 jellyfishes, molluscs, annelids, large protists and a few copepod families. The attenuation rate
39 of vertical particle fluxes was weaker at such oxygen-depleted sites. Canonical redundancy
40 analyses showed that the epipelagic zooplankton community composition depended on the
41 community structure of surface phytoplankton and the quantity and the quality of the produced
42 particulate organic matter. We provide a consistent baseline of plankton community structure
43 together with estimates of vertical flux and a contribution to our understanding of global
44 zooplankton dynamics in the upper kilometer of the global ocean. Our results further suggest
45 that future changes in surface phytoplankton composition and mesopelagic oxygen loss might
46 lead to profound changes in zooplankton abundance and community structure in both the
47 euphotic and mesopelagic ocean. These changes may affect the vertical export and hereby the
48 strength of the biological carbon pump

49
50
51 **Keywords: Zooplankton, Global Ocean, biological carbon pump, Epipelagic, Mesopelagic, Community**
52 **structure, Particle flux, Attenuation rates, Oxygen Minimum Zone.**

Introduction

The upper kilometer of the ocean constitutes a habitat where most of the organic carbon produced by the phytoplankton in the epipelagic layer (0-200m) sinks into the mesopelagic layer (200-1000m) while being progressively consumed and respired. Within the wide size spectrum of planktonic organisms (0.02μm-2m), mesozooplankton (0.2-20mm) are a pivotal component of marine trophic webs impacting the Biological Carbon Pump (BCP) through their feeding, vertical migration, and the production of faecal pellets (Steinberg and Landry, 2017). In a context of global climate change, zooplankton communities experience increasingly stressful conditions through global warming, ocean acidification and deoxygenation (Oschlies et al., 2018; Schmidtko et al., 2017), enhanced water column stratification in the open ocean and modifications in phytoplankton production and community structure (Coma et al., 2009; Kwiatkowski et al., 2019; Richardson, 2008). Long term field surveys have shown how shifts in climatic conditions lead to large shifts in surface zooplankton composition (Beaugrand et al., 2019). Future climate warming could further reduce macronutrient supplies in the upper ocean and therefore decrease phytoplankton biomass in the tropical open ocean or can cause positive trophic amplification in the polar ocean (Chust et al., 2014). Such changes in biomass may be amplified in the zooplankton through trophodynamic effects, which could greatly alter the fluxes of organic matter into the deeper mesopelagic layers. Within the latter, modifications of the quantity and quality of the vertical particle flux produced in the surface layers could trigger substantial changes in mesozooplankton abundance and composition. In addition, the expansion of Oxygen Minimum Zones (OMZ) (Schmidtko et al., 2017; Stramma et al., 2010) may further constrain the spatial distribution of the numerous zooplankton taxa that are sensitive to dissolved oxygen levels (Ekau et al., 2010; Kiko et al., 2020; Kiko and Hauss, 2019; Seibel, 2011; Wishner et al., 2020, 2018). Therefore, understanding the variations of zooplankton biomass and diversity in the epi and mesopelagic is essential to better understand the impact of global climate change on the properties of marine ecosystems.

However, mesopelagic zooplankton communities remain critically under-sampled compared to the epipelagic ones, as most collections is in the first 200m of the water column (Everett et al., 2017). The mesopelagic is still considered a "dark hole" (Robinson et al., 2010; St John et al., 2016) as the gaps in sampling lead to critical gaps in knowledge regarding the functioning of mesopelagic ecosystems and how they are controlled by the organic matter fluxing from the euphotic zone. Local to regional field studies reported that the abundance of mesozooplankton decreases exponentially with depth, in parallel with substantial changes in species diversity and genus composition that remain poorly resolved (Bode et al., 2018;

87   Brugnano et al., 2012; Hernández-León et al., 2020; Koppelmann et al., 2005; Kosobokova and

88   Hopcroft, 2010; Yamaguchi et al., 2004). Some studies reported increases in diversity with

89   depth, with maxima in the meso- to bathypelagic layers (Bode et al., 2018; Gaard et al., 2008;

90   Kosobokova and Hopcroft, 2010; Yamaguchi et al., 2004), whereas other studies reported either

91   the opposite diversity pattern or even an absence of vertical patterns due to large spatio-

92   temporal variability (Gaard et al., 2008; Hidalgo et al., 2012; Palomares-García et al., 2013;

93   Wishner et al., 2008). Such mismatch between observations might be related to the wide range

94   of environmental conditions sampled using a variety of sampling gears that make inter-

95   comparisons difficult. One recent global analysis of zooplankton vertical distribution in inter-

96   tropical regions showed that in this narrow latitudinal band the vertical dimension was the main

97   structuring pattern suggesting that midwater processes mediated by zooplankton may not

98   change between oceans at those latitudes (Fernández de Puelles et al., 2019). How these

99   changes relate to the vertical flux and also across the full latitudinal band is poorly understood

100   because plankton observations and biogeochemical studies have usually been carried out by

101   distinct scientific communities. Recent interdisciplinary cruises have taken place, providing

102   more integrated knowledge on the importance of zooplankton to carbon sequestration (Guidi et

103   al., 2016; Kiko et al., 2020; Steinberg and Landry, 2017; Stukel et al., 2019). No global study

104   has yet been able to analyse community-level variations in zooplankton abundances, biomass

105   and community composition in conjunction with assessments of vertical particle flux in the

106   upper kilometre of the global ocean.

107   Here, a homogeneous dataset of community-level zooplankton images generated from

108   the TARA Oceans expeditions is explored together with associated measurements of their

109   contextual environmental conditions to: (i) test whether zooplankton communities present

110   consistent vertical variations in abundance and composition across the oceans and in different

111   latitudinal bands, and (ii) investigate the main drivers of such vertical gradients and how they

112   are coupled to the surface phytoplankton and estimates of particle flux. The TARA Oceans

113   expedition collected over 35000 samples encompassing the whole plankton community (i.e.,

114   from viruses to jellyfish) across the global ocean from 2009 to 2013 (Karsenti et al., 2011).

115   Previous studies that analysed the TARA Oceans imaging dataset explored the global latitudinal

116   gradients in richness and composition for the whole plankton community focusing on surface

117   waters (Ibarbalz et al., 2019; Brandao et al., in press). Here, we aim to describe the community

118   composition of mesozooplankton down to 1000m depth on a global scale. As the imaging

119   techniques used here cannot achieve a species-level identification of the zooplankton

120   community composition, our approach is rather oriented towards larger taxonomic and /or

121   functional groups that may be associated with broad ecological and biogeochemical functions.

122   ## Materials and methods

123   **Sampling sites and environmental variables**

124   TARA Oceans took place between 2009 and 2013. Among the 210 stations that were

125   sampled, 57 stations covering 7 ocean basins (Fig. 1) were sampled with a Multinet (Pesant et

126   al., 2015; Roullier et al., 2014), a sampling device with five nets that allows for depth-stratified

127   sampling (see below).
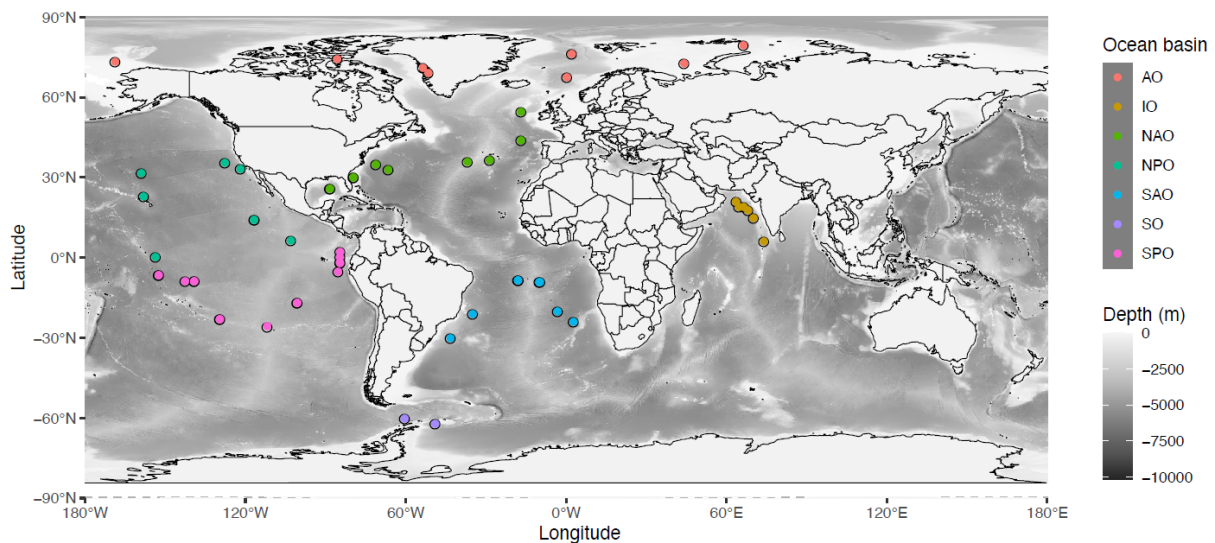
128

129   Fig. 1: Location of the 57 stations sampled with the Multinet, grouped by ocean basin: AO=Arctic

130   Ocean, IO=Indian Ocean, NAO=North Atlantic Ocean, NPO=North Pacific Ocean, SAO=South

131   Atlantic Ocean, SO=Southern Ocean or Austral Ocean, SPO=South Pacific Ocean.

132

133   A CTD rosette equipped with optical sensors was deployed to measure the physico-

134   chemical parameters within the water column. Temperature and conductivity were measured

135   from the surface to a maximum of 1300 m depth using a Seabird 911 CTD mounted on a Sea-

136   Bird Carousel sampler with 10 Niskin bottles. The following additional sensors were mounted

137   to measure optical properties related to relevant biogeochemical variables: fluorometer (Wetlab

138   ECO-AFL/FL model), dissolved oxygen sensor (model SBE 43), nitrate sensor (ISUS with a

139   maximum rating depth of 1000m Satlantic SA), a 25 cm transmissometer for particles 0.5–20

140   μm (WETLabs), a one-wavelength backscatter meter for particles 0.5–10 μm (WETLabs), and

141   an Underwater Vision Profiler 5 (UVP5) for particles >150 μm and zooplankton >600 μm

142   (Hydroptic). Assuming that particle sinking speed increases with size, those particles detected
143   through the backscattering will be referred to as suspended particulate matter (SPM, particles
144   < 10µm in Equivalent Spherical Diameter), while the ones detected by the UVP5 (>150µm in
145   Equivalent Spherical Diameter) will be referred as particles. Vertical particle mass flux (in mg
146   Dry Weight m^{-2}d^{-1})) was calculated from the particle size spectra detected by the UVP5 as in
147   (Guidi et al., 2008). Based on the High Pressure Liquid Chromatography (HPLC) analysis of
148   water collected with Niskin bottles, we used the method of Uitz et al. (2006) to estimate the
149   contribution (%) of three pigment size classes (microphytoplankton, nanophytoplankton, and
150   picophytoplankton; $f_{\_micro}$, $f_{\_nano}$, and $f_{\_pico}$, respectively) to total phytoplankton biomass in
151   the epipelagic layer. The median value of all hydrological and optical data together with
152   imaging data were calculated for each of the five horizontal layers sampled by the Multinet for
153   future data processing. The samples were classified as anoxic, hypoxic and normoxic according
154   to the oxygen minimum value measured within the towed layer. We used a threshold of
155   5 $\mu mol\ kg^{-1}$ to classify the stations as anoxic (Roullier et al., 2014) and 58.5 $\mu mol\ kg^{-1}$(Bode
156   et al., 2018) to classify them as hypoxic.

Zooplankton sampling, digitization, biomass estimates

158   A Hydrobios Multinet (with a 300µm mesh and an aperture of 0.25m^2) was used to
159   sample zooplankton (Roullier et al., 2014; Pesant et al., 2015) in five distinct water layers
160   ranging from the surface to occasionally 1300 m depth. The five depth layers were locally
161   defined as a function of the vertical structure of the water column according to the profiles of
162   temperature, salinity, fluorescence, nutrients, oxygen, and particulate matter (Pesant et al.,
163   2015). The Multinet was equipped with a flowmeter to measure the volume of seawater filtered
164   by each net tow (Pesant et al., 2015). Day and night net tows were conducted at ten stations.
165   Sampling at the other stations occurred at day or night, depending on cruise schedule and
166   operational constraints. Once collected, the samples were preserved in a solution of buffered
167   formaldehyde-Borax solution (4%). In the laboratory, the samples were rinsed and split with a
168   Motoda box (MOTODA, 1959). The final split was analysed with the Zooscan imaging system
169   (Gorsky et al., 2010) which allowed a rapid and semi-automatic analysis of zooplankton
170   samples. In total, the samples comprised nearly 400,000 images of living zooplankton and
171   detritus. These images were imported into Ecotaxa, an online platform which allows an
172   automatic prediction of the taxonomic classification of each single image followed by a manual
173   validation/correction. The organisms were then identified manually down to the order,
174   sometimes to the family and rarely down to the genus level. All copepods were sorted at the

175 family level apart from the smallest copepods that cannot be recognised at the family level from

176 the image. They were all grouped into one category called Other-copepoda or other-Calanoida

177 if their morphological features allowed classifying them as Calanoida. This initial sorting

178 allowed classifying zooplankton into 119 taxa. As many taxa showed a very small contribution

179 to total zooplankton abundance, the 119 taxa were grouped into 19 taxonomic groups (Table

180 1). Those include all the major zooplankton groups that are frequently observed in the oceans.

181 To investigate vertical patterns in mesozooplankton abundance, these 19 groups were further

182 aggregated into eight groups representing a combination of taxonomic and functional

183 classification (Table 1).

184 Once the zooplankton images were sorted, Ecotaxa enabled us to extract the

185 concentration and the biovolume of each mesozooplankton group at every station and for every

186 net tow, while accounting for the Motoda fraction and the volume sampled. The biovolume was

187 computed for each individual zooplankton using the minor and major length axes assuming a

188 prolate ellipsoidal shape (Gorsky et al., 2010). The biomass was calculated for the 8 large

189 groups using the equations for the different taxa :

190 $$Body\ Weight(\mu C) = aS^b \tag{1}$$

191 where S is body area in mm^2. Taxon-specific area-to-dry mass conversion factors

192 (Lehette and Hernandez-Leon, 2009) and dry mass to carbon (C) conversion factors (Kiørboe,

193 2013) were used to calculate the biomass and C content of each zooplankton organism scanned.

194 Taxonomic units and biomass conversion factors used are listed in Table 2. For large protists

195 the conversion factor was adjusted to 0.08 $mgC\ mm^{-3}$ (Biard et al., 2016).

196 Shannon diversity index (H') was calculated based on the relative abundances of the

197 119 taxa for each sample as follows:

198 $$H' = -\sum_{i}^{n}\ p_i log p_i \tag{2}$$

199 where p_i is relative abundance of each taxa in one sample and log is the natural

200 logarithm.

201

Analyzing zooplankton and particles vertical distributions

203 Vertical attenuation rates of zooplankton (abundance and biomass) and estimated

204 particle fluxes were estimated, from the five sampled layers for zooplankton and from the 5

205 meter resolution profile of estimated vertical flux using a linear regression of the log-log (i.e.

206 natural logarithm) with the following equation :

207 $$X = X_0(Z/Z_0)^b \tag{3}$$

208   where X represents the zooplankton abundance, the zooplankton biomass or the
209   particle vertical flux at the depth level Z, X_0 the zooplankton biomass or abundance and vertical
210   particle flux at the depth Z_0 (chosen as median depth of the surface net) and b the slope taken
211   as a proxy of the attenuation rate of zooplankton biomass zooplankton abundance or particle
212   flux. In the rest of the manuscript, A_zoo represents the slope b of vertical profile for
213   zooplankton abundance, B_zoo the slope b of vertical profile for zooplankton biomass, A_flux
214   the slope b of vertical profile for particle flux, and P_flux1, P_flux2 and P_flux3 the particle
215   flux in respectively the epipelagic, upper and lower mesopelagic. To analyse latitudinal patterns
216   in attenuation rates, the slope values were separated into three latitudinal bands based on the
217   latitudinal position of their corresponding sampling stations: intertropical (0°-30°), temperate
218   (30-60°) and polar (60°-90°). The intertropical stations gathered both OMZ and non-OMZ
219   stations, which allowed us to analyse the effect of oxygen depletion on zooplankton and
220   particles. Non-parametric variance analyses (Kruskal and Wallis tests) were performed to test
221   for differences in slope values (i.e. zooplankton and particles attenuation rates) between
222   latitudinal bands.

Multivariate analysis of community composition

224   To explore the response of zooplankton community composition to environmental
225   drivers across depth layers, the non-interpolated abundances of the 19 taxonomic groups
226   mentioned above were aggregated into three layers: the epipelagic layer (0-200m), the upper
227   mesopelagic layer (200-500m) and the lower mesopelagic layer (500-1000m). To analyse
228   separately the three depth layers, the samples collected in overlapping layers (18.59% of the
229   total samples) were not included in the statistical analysis (Table S1). To characterise the
230   environmental conditions of each layer at each sampling station the median values of the
231   following contextual environmental variables were used: temperature (T), salinity (S), oxygen
232   (O_2), nitrate concentration (NO_3), chlorophyll a concentration (Chl_a), phytoplankton size
233   fractions (f_{micro}, f_{nano}, and f_{pico}), concentration of suspended particles (SPM) and particle
234   flux (P_Flux). The measurements of all these environmental variables are available on
235   PANGAEA (https://doi.org/10.1594/PANGAEA.840721).

236   To estimate the strength of the Diel Vertical Migration (DVM) at 10 stations, pairwise
237   Wilcoxon tests were performed to compare in each layers the abundance and biomass of each
238   taxa between day and night. For those 10 same pairs of stations, we used an analysis of
239   similarities (ANOSIM) to test for significant variations in community composition between day
240   and night samples. The ANOSIM tested whether the inter-groups difference (day and night

241   groups) was higher than the intra-groups difference, by providing an R coefficient. An R
242   coefficient close to one suggests dissimilarity between groups, while R value close to zero
243   suggests an even distribution of high and low ranks within and between groups. An R value
244   below zero suggests that dissimilarities are greater within groups than between groups (Clarke
245   and Gorley, 2001). ANOSIM tests were performed within each layer using log-transformed
246   (where log is the natural logarithm) abundances and Bray-Curtis distance among stations.

247   For each depth layer, a canonical redundancy analysis (RDA) was performed based on
248   the abundances of the 19 mesozooplankton groups and the above-mentioned environmental
249   variables to explore the explanatory power of these variables in structuring the
250   mesozooplankton community. The RDA is an extension of the multiple regression analysis
251   applied to multivariate data (Legendre and Legendre, 1998). It allows representing the response
252   variables (abundances of the 19 mesozooplankton groups) in a "constrained" reduced space,
253   i.e., constructed from the explanatory variables (the environmental variables). For each RDA,
254   the following variables were used as "supplementary variables" of the analysis in order to
255   visualize their correlation with the environmental structuring of the mesozooplankton
256   community (i.e., to visualise their position in the RDA space): attenuation of particle flux
257   (A_flux), attenuation of zooplankton abundance (A_zoo), attenuation of zooplankton biomass
258   (B_zoo) and the Shannon index (H'). Beforehand, a Hellinger transformation was performed
259   on the mesozooplankton abundances. A preliminary RDA based on all samples together showed
260   a very strong effect of depth on mesozooplankton community composition (Fig. S1). Therefore,
261   to avoid such a strong effect of depth on the community composition analysis, three separate
262   RDAs were performed on each of the three layers defined above. Significant axes were
263   identified using the Kaiser-Guttman criterion (Legendre and Legendre, 1998).

264   Data manipulation and statistical analyses were performed with Matlab 2018b
265   (MATLAB 9.5) for the vertical profiles of abundance and biomass and statistical test (Wilcoxon
266   test, Kruskal-wallis test), R environment v3.5.1 (using the following packages: vegan version
267   2.5-5, ggplot2 version 3.1.1, ggrepel version 0.8.0 and ggfortify version 0.4.7) for the
268   redundancy analysis and PRIMER6 (Version 6.1.12) and PERMANOVA+ (Version 1.0.2) for
269   the ANOSIM test.

270   ## Results

271   **Day night variability**

272   In each layer, the comparison between day/night of the taxonomic groups indicated that
273   only a few groups (Euphausiidae, Metridinidae, Corycaeidae and Cnidaria for abundance;
274   Eumalacostraca and Ostracoda for biomass) showed significant differences in either the surface
275   layer or the upper mesopelagic layer (Table S1). Nonetheless, the ANOSIM found no
276   significant differences in the community composition between the day and night samples at the
277   community-level (R0-200m = -0.039; R200-500m = -0.008; R500-1100m = -0.006). The same
278   analyses based on biomass also indicated no significant differences (R0-200m = 0.018; R200-
279   500m = -0.051; R500-1100m = 0.087). As a consequence, all further analyses were carried out
280   without making any distinctions between day and night samples.

281   **Vertical patterns in zooplankton total abundance and biomass and particle flux**

282   On a global scale, zooplankton abundance and biomass decreased exponentially with
283   depth (Fig. 2) in the different latitudinal bins. Abundance and biomass decrease rate with depth
284   and were correlated ($r2=0.342$, $p=4.6 \times 10^{-5}$) but the biomass attenuation rate estimates were
285   systematically lower than the attenuation based on the abundance profiles. On average, polar
286   waters showed increased zooplankton abundance and biomass compared to the stations located
287   in the tropics. In the epipelagic layer, abundances and biomass ranged from 1 to 5000 ind m^{-3}
288   and 0.05 to 200 mg C m^{-3} while in the mesopelagic they were reduced to 0.05 to 450 ind m^{-3}
289   and 0.005 to 40 mg C m^{-3}. Copepods were the most abundant being 85% and 65% of the
290   abundance and biomass in the epipelagic, 85 and 76% in the upper mesopelagic and 95% and
291   97% in the lower pelagic (Table 3). The estimated vertical flux also decreased with depth in all
292   latitudinal bands. On average polar waters showed higher fluxes compared to the stations
293   located in the tropics.

294
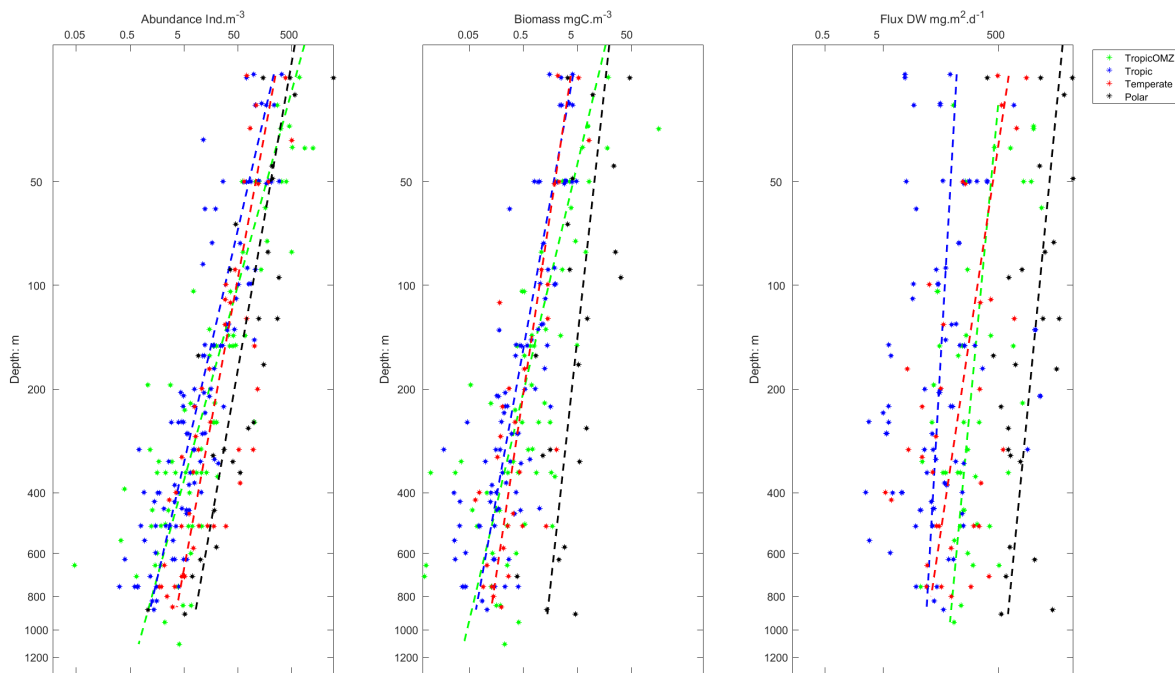
Fig. 2: Vertical distribution of zooplankton biomass, abundance and particle flux in different latitudinal bands. Dotted lines represent the fitted linear regression for each latitudinal band (equation 3). The linear fits to the data point are given in table 4.

The attenuation rates of zooplankton abundance and biomass with depth were stronger than the attenuation rates of the vertical particle flux (Fig. 3A, B and C, Table 4). The decrease rates in zooplankton vertical abundance and biomass are more pronounced in OMZ stations compared to the non-OMZ stations. Yet, such difference was found to be significant only when the vertical decrease rates were calculated from abundances. In general, zooplankton attenuation rates decreased with latitude whereas the attenuation rates of particle fluxes increased with latitude (Fig. 3, Table 3). A non-parametric variance analysis (Kruskal-Wallis test) of the attenuation rate revealed significant differences in the attenuation rates of zooplankton abundances between the anoxic tropical stations and the temperate and polar ones, but not with the other tropical stations (Table 4). No statistical difference between regions was found. The attenuation rate of vertical flux was weaker at the OMZ sites compared to the non OMZ ones but this difference was not significant (Fig. 3B).
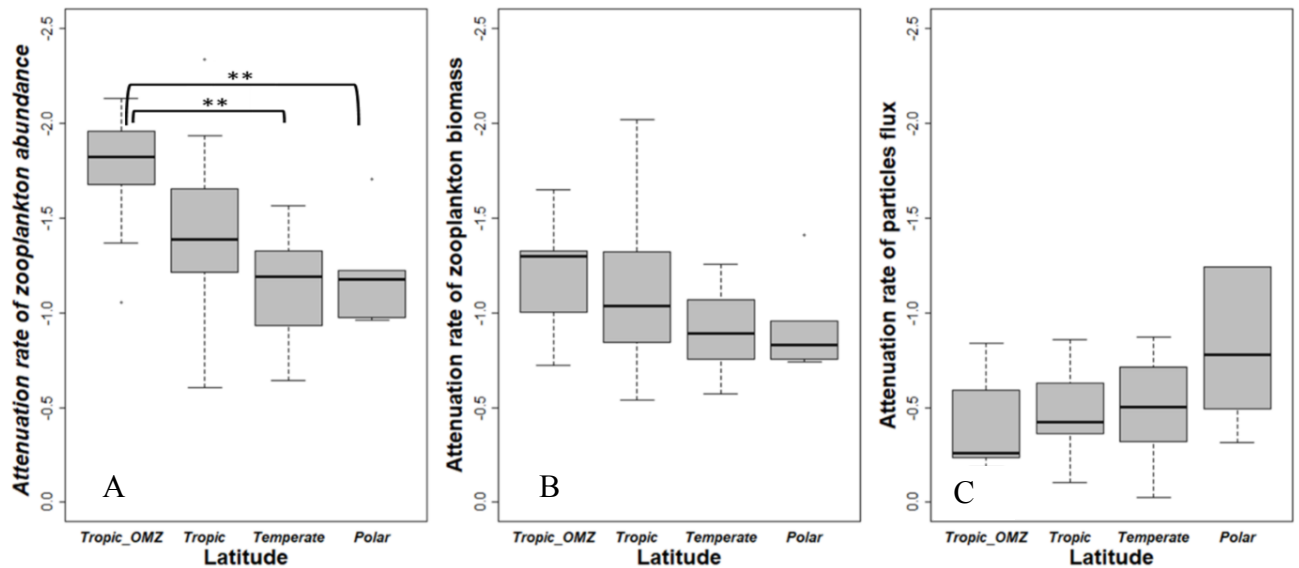
312
313   Fig. 3: Distributions of attenuation rates at each station per latitudinal bands (Tropical, Tropical
314   OMZ, Temperate, and Polar). A: Attenuation rate of zooplankton abundance (A_zoo). B: Attenuation
315   rate of zooplankton biomass (B_zoo). C: Attenuation rate of particle flux (A_flux). (**) means
316   significant Kruskal-Wallis test with $p < 0.01$ (Table 5).

317

318   **Structuring of the epipelagic community composition.**

319   In the epipelagic layer (0 – 200 m depth), the environmental variables explained 32.71%
320   of the total variance in mesozooplankton groups' abundances. The first RDA axis (RDA1, 57.18
321   % of constrained variance) opposed the samples from polar waters, and especially those from
322   the Arctic dominated by Calanidae and crustacean larvae (RDA1 > 0), to the tropical samples
323   presenting more even contributions from most of the remaining groups: Protista,
324   Eumalacostraca, Annelida, Amphipoda, Corycaeidae, Chaetognatha, Euphausiacea,
325   Oithonidae, Ostracoda, Oncaeidae, Calanoida (RDA1 < 0). RDA1 was negatively scored by
326   temperature and salinity and positively scored by vertical particle flux, microphytoplankton
327   contribution, suspended particle concentration, dissolved oxygen concentration and chlorophyll
328   *a* concentration. Among the supplementary variables, the attenuations of the particle flux and
329   of the zooplankton biomass were positively correlated with RDA1, while the attenuation of the
330   zooplankton abundance and the Shannon index were negatively correlated to RDA1. RDA2
331   (13.1% of constrained variance) opposed the samples from the Indian Ocean and North Atlantic
332   Ocean that present higher abundances of Cnidaria, Mollusca, Tunicata and Cladocera (RDA2
333   < 0) to those samples from the Southern Ocean presenting higher abundances of Annelida,
334   Euphausiacae, Amphipoda and Other Copepoda (RDA2 > 0). RDA2 was positively scored by

335   nitrate concentrations and the relative contribution of nanophytoplankton. It was negatively

336   scored by the concentration of suspended particles and the relative contribution of

337   microphytoplankton. All supplementary variables were negatively correlated with RDA2.
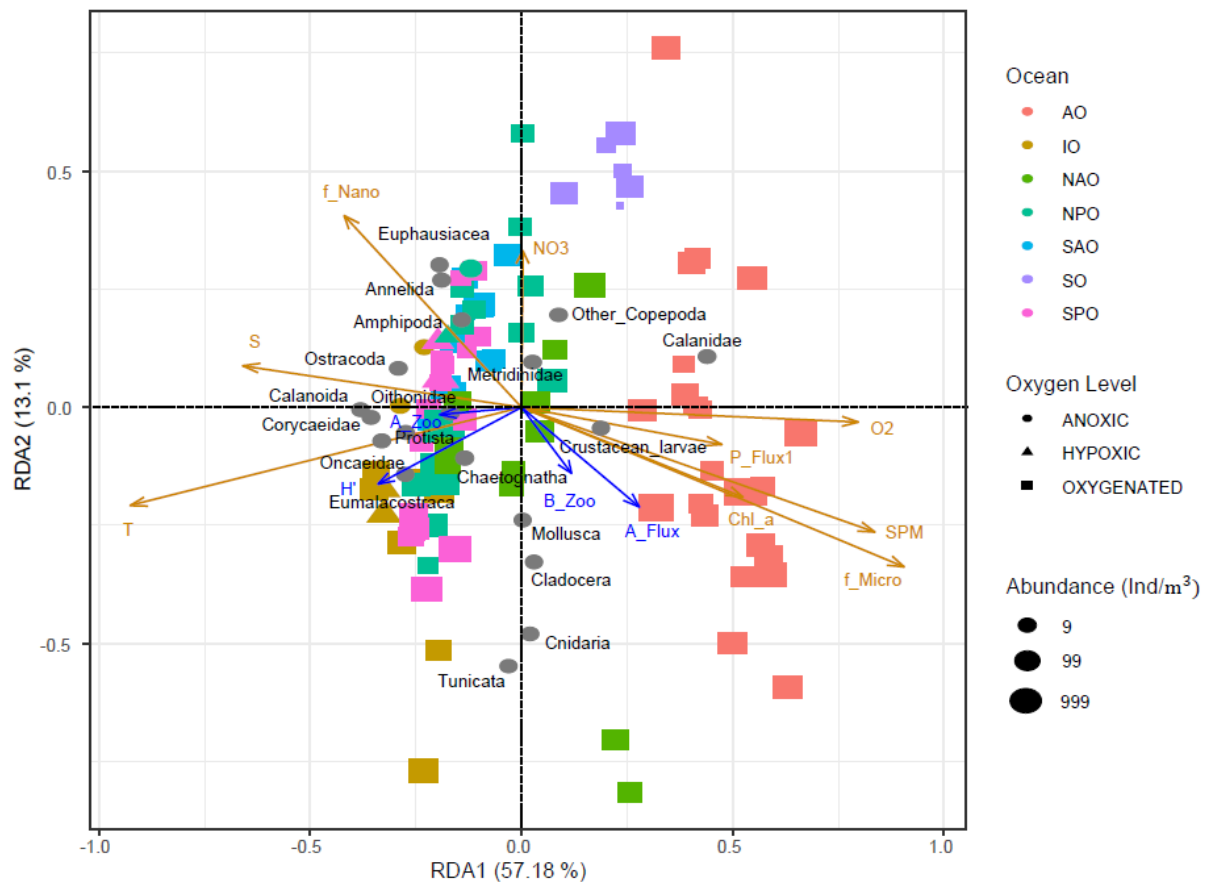
338
339   Fig. 4: RDA on the epipelagic communities. Each dot corresponds to a sample, i.e., one net at one depth

340   at one station. The orange arrows correspond to the quantitative environmental variables in RDA space:

341   f_pico, f_nano and f_micro correspond to the relative contribution (%) of pico-, nano- and micro-

342   phytoplankton to total phytoplankton biomass, O2 = dissolved oxygen concentration (μmol/kg), Chl_a

343   = Chlorophyll a concentration (mg/m3), SPM = suspended particles matter (m/sr), T = temperature (°C),

344   Sal = salinity, NO3 = nitrate concentration (mol/kg), Z = depth (m)) and P_Flux= particulate flux

345    $(mg.m^{-2}.d^{-1})$. Grey dots mark the projection of the zooplankton groups abundance $(ind.m^{-3})$. Colors

346   correspond to the ocean basin where the samples were taken: AO = Arctic Ocean, IO = Indian Ocean,

347   NAO = North Atlantic Ocean, NPO = North Pacific Ocean, SAO = South Atlantic Ocean, SO = Southern

348   Ocean, SPO = South Pacific Ocean. Shapes illustrate oxygen level, Anoxic: $[O_2]$ <5μmol/kg; Hypoxic:

349   5μmol/kg< $[O_2]$ <58.5μmol/kg and oxygenated: $[O_2]$>58.5μmol/k). Supplementary variables estimated

350   for the epipelagic layer are represented with blue arrows: attenuation of particle flux (A_flux),

351   attenuation of zooplankton abundance (A_zoo), attenuation of zooplankton biomass (B_zoo) and the

352   Shannon index (H').

Structuring of the upper mesopelagic community composition.

In the upper mesopelagic layer (200 to 500 m depth), the environmental variables explained 29% of the total variance in mesozooplankton groups' abundances. Again, the first RDA axis (RDA1, 36.33% of constrained variance) mainly opposed the polar samples dominated by Calanidae copepods, and characterized by higher concentrations of suspended particle, particle flux (both from surface and upper mesopelagic layer), and higher dissolved oxygen concentrations (RDA1 > 0), from the samples characterized by more diverse zooplankton communities (mainly Corycaeidae, small Calanoida, Oncaeidae) and correlated to higher temperature, higher salinity and a higher relative contribution of the nanophytoplankton (RDA1 < 0). Similarly, to what was observed for the epipelagic layer, among the supplementary variables, the attenuations of the particle flux and of zooplankton biomass were positively correlated with RDA1, while the attenuation of zooplankton abundance and the Shannon index were negatively correlated to RDA1. RDA2 (24.72% of constrained variance) opposed the anoxic samples from the Indian Ocean presenting higher abundances of Tunicata, Annelida, Protista, Mollusca, Oithonidae and Cnidaria (RDA2 < 0) to the oxygenated ones displaying higher abundances of Ostracoda, Eumalacostraca, crustacean larvae, other Copepoda, Chaetognatha and Euphausiacea (RDA2 > 0). Samples from the Arctic Ocean were dominated by large copepods from the Calanidae and Metridinidae families. Samples from the Pacific and Atlantic Oceans were dominated by other Copepoda, Eumalacostraca, Ostracoda, Euphausiacea, Chaetognatha and crustacean larvae. Higher attenuation rates of zooplankton biomass and particle flux were found in polar samples whereas higher zooplankton attenuation rates were found in warmer waters, especially at OMZ stations. Again, samples from the tropical upper mesopelagic layers displayed more diverse communities. The distribution of the supplementary variables along RDA2 differed from what was observed for the epipelagic layer, as the supplementary variables, except the attenuation of the zooplankton abundances, were positively correlated to RDA2.
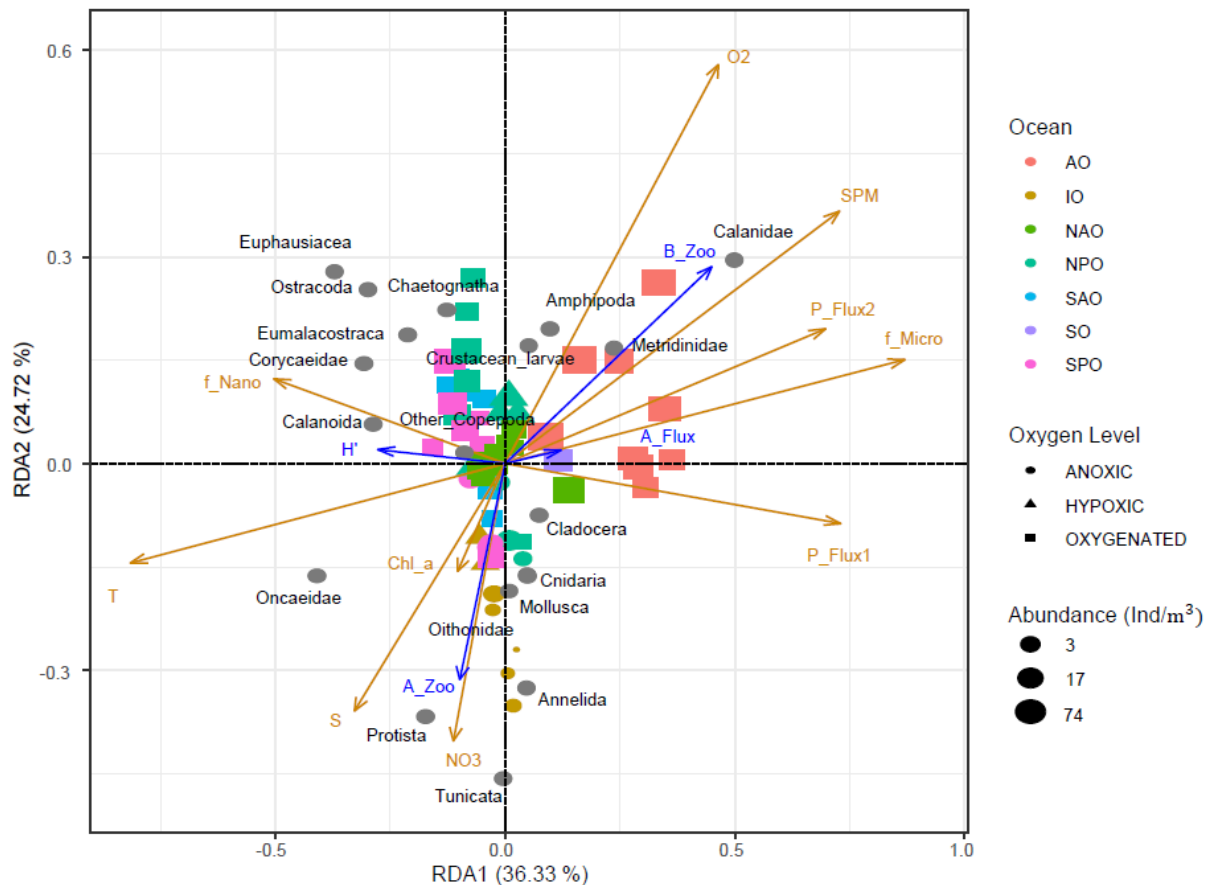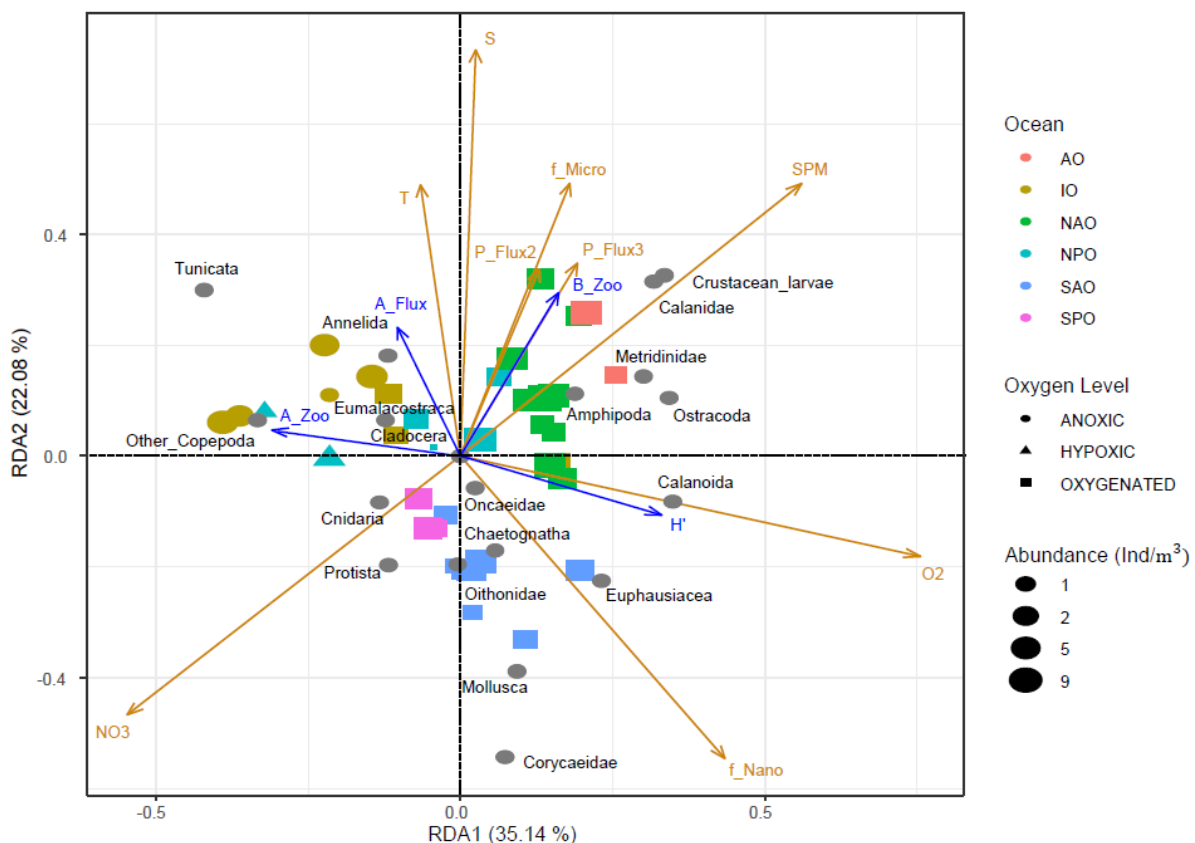
Fig. 5: RDA performed on the upper mesopelagic abundances. Each dot corresponds to a sample, i.e., one net at one depth at one station. The orange arrows correspond to the quantitative environmental variables (see legend of Fig. 4). Anoxic: $[O_2]$ <5µmol/kg; Hypoxic: 5µmol/kg< $[O_2]$ <58.5µmol/kg and oxygenated: $[O_2]$>58.5µmol/kg). Supplementary variables estimated for the upper mesopelagic layer are represented with blue arrows: attenuation of particle flux (A_flux), attenuation of zooplankton abundance (A_zoo), attenuation of zooplankton biomass (B_zoo) and the Shannon index (H').

Structuring of the lower mesopelagic community composition

In the lower mesopelagic layers (500 to 1000 m depth), the environmental variables explained 29.46 % of the total variance in mesozooplankton groups' abundances. The first RDA axis (RDA1, 35.14 % of constrained variance) opposed the stations from the Arctic and North Atlantic Oceans characterized by higher dissolved oxygen concentrations, higher suspended particle concentrations (RDA1 > 0), from the anoxic and nitrate-rich stations from the Indian Ocean (RDA1 < 0). The former stations were characterized by higher abundances of Calanidae, Calanoida, Metridinidae, crustacean larvae, Ostracoda and Amphipoda, whereas the latter were characterized by higher abundances of Tunicata, Annelida, Eumalacostraca and other Copepoda. RDA2 (22.08 % of constrained variance) separated the colder and less salty stations of the Southern Atlantic Ocean (RDA2 < 0) from the warmer, saltier stations (RDA2 > 0) of

397   the North Atlantic and the Indian Oceans that are characterized by less diverse zooplankton

398   communities. The stations that sampled the oxygenated waters of the North Atlantic and Arctic

399   Oceans were dominated by large copepods of the Metridinidae and Calanidae families, as well

400   as most of the small other Calanoida (i.e. those smaller copepods that could not recognized at

401   a more detailed taxonomic level) in addition to Ostracoda, Amphipoda, and crustacean larvae.

402   Oxygenated stations from the South Atlantic Ocean (SAO) were characterized by higher

403   abundances of Chaetognatha, Corycaeidae, Euphausiacea, Cnidaria, Mollusca, Oithonidae,

404   Oncaeidae and Protista. Samples taken in the OMZ of the Indian and North Pacific Oceans

405   displayed higher abundances of other Copepoda, Tunicata, Annelida, Eumalacostraca and

406   Protista. Higher mesozooplankton biomass and stronger particle flux attenuation rates were

407   found in the normoxic waters while higher zooplankton attenuation rates were observed at the

408   stations that sampled an OMZ. The distribution of the supplementary variables showed similar

409   association with environmental variables as in the upper mesopelagic.

410

Fig. 6: RDA performed on the lower mesopelagic abundances. Each dot corresponds to a sample, i.e., one net at one depth at one station. The orange arrows correspond to the quantitative environmental variables (see legend of Fig. 4). Anoxic: $[O_2]$ <5µmol/kg; Hypoxic: 5µmol/kg< $[O_2]$ <58.5µmol/kg and oxygenated: $[O_2]$>58.5µmol/kg). Supplementary variables estimated for the lower mesopelagic layer

416   are represented with blue arrows: attenuation of particle flux (A_flux), attenuation of zooplankton

417   abundance (A_zoo), attenuation of zooplankton biomass (B_zoo) and the Shannon index (H').

418

419

420 **Discussion**

421   The present global analysis of spatial patterns of the mesozooplankton community and

422 their relationship with the strength of the vertical particle flux is based on zooplankton

423 abundance and biomass estimates and vertical particles flux estimated using state-of-the-art

424 imaging techniques (Zooscan and UVP5). The rigorous quality control (see Supplementary

425 Material) allows to depict with confidence correlations between zooplankton and particle flux,

426 two important components of the biological carbon pump (BCP). Notably the study allows to

427 infer global ecological patterns in the epipelagic and mesopelagic layers, the coupling between

428 these two layers in oxygenated, hypoxic and anoxic situations.

429 **Important environmental factors for the mesozooplankton community composition in the**
430 **epipelagic layer**

431   High latitude marine ecosystems are characterised by a combination of lower species

432 diversity and shorter food webs (Laws, 1985; Stempniewicz et al., 2007) sustained by higher

433 concentrations of large microphytoplankton cells (diatoms). On the contrary, low latitude

434 ecosystems are featured by more complex and diverse food webs (Saporiti et al., 2015; Uitz et

435 al., 2006) adapted to lower production rates ensured by smaller cells (i.e. pico- and

436 nanoplankton). How the dynamics of zooplankton community composition and vertical particle

437 flux follow this scheme remains more elusive. Previous field-based studies reported peaks in

438 zooplankton species richness in the tropics (Rombouts et al., 2010; Rutherford et al., 1999;

439 Yasuhara et al., 2012), which is in line with the above-mentioned theory that the tropical food-

440 depleted regions promote more complex food-webs with higher species richness. Our RDAs

441 results result supports the view that, on a global scale, temperature and the production regime

442 of surface ecosystems are the main drivers of zooplankton community structure in the

443 epipelagic layer. Therefore, our observations fall in line with the theory described above: in the

444 epipelagic layers, less abundant and more diverse zooplankton thrive in warm, pico- and

445 nanophytoplankton-dominated waters contrary to the polar waters where zooplankton is much

446 more abundant but less diverse. Polar waters are characterised by a higher contribution of

447 microphytoplankton to total phytoplankton biomass and higher concentrations of particles. Our

448 results also indicate that the two polar communities are not completely alike, as the Arctic is

449 dominated by calanoid copepods while euphausiids and small undetermined copepods

450 dominate in the few stations sampled in the Southern Ocean. Such differentiation has been

451 previously shown by several authors who found that Arctic zooplankton were dominated by

452 *Calanus* spp. (Balazy et al., 2018; Hirche and Mumm, 1992), whereas it was shown that

453   Antarctic zooplankton were dominated by euphausiids, small calanoids, cyclopoids (i.e.

454   *Oithona* spp., *Oncaea* spp.) and salps (Park and Wormuth, 1993; Quetin et al., 1996; Ross et

455   al., 2008).

Important environmental factors for the mesozooplankton community structure in the mesopelgic layer

458   The RDA displayed similar general patterns in both the upper and lower mesopelagic

459   layers with the stations in the Indian Ocean (with low zooplankton concentration in low oxygen)

460   and Arctic Ocean (with high zooplankton concentration in oxygenated conditions) being in all

461   layers well separated from the other stations in the remaining ocean. The highest mesopelagic

462   zooplankton concentrations were found at stations associated with high microphytoplankton

463   concentrations in the epipelagic and high particle flux, suggesting a strong impact of surface

464   production regime on the mesozooplankton in the mesopelagic (Hernández-León et al., 2020).

465   The inter-basin differences in zooplankton concentration and community composition was

466   slightly lower in the lower mesopelagic compared to the upper mesopelagic, probably due to

467   the more homogeneous habitat (Fernández de Puelles et al., 2019).

468   In general, stations associated with anoxic or hypoxic conditions at midwater depth

469   displayed lower zooplankton concentrations in the mesopelagic and different community

470   composition from oxygenated layers. The stations that sampled the tropical OMZ showed

471   higher proportions of gelatinous carnivorous zooplankton (Cnidaria), gelatinous filter feeders

472   (Tunicata), Mollusca and small omnivorous grazers (Cladocera). Anoxic or strongly hypoxic

473   conditions in the mesopelagic may have selected for those taxa adapted to low oxygen (Vaquer-

474   Sunyer and Duarte, 2008). In mesopelagic oxygenated waters, the stations of the Tropical

475   Pacific Ocean displayed a higher diversity stemming from the higher and relatively even

476   abundances of large protists (i.e. Rhizaria and Foraminifera), chaetognaths, crustaceans

477   (Ostracods, Euphausiacea, Eumalacostraca, Amphipoda), and various copepod families

478   (Corycaeidae, Oithonidae, Oncaeidae, small Calanoida). These zooplankton communities were

479   associated with oligotrophic conditions at surface (Fig. 4), lower zooplankton abundances,

480   lower concentrations of suspended matter, weaker particle fluxes and weaker attenuation rates

481   (Fig. 3B) and with stronger attenuation rates of organisms' abundances (Fig. 3A). Therefore,

482   we evidence oligotrophic regimes where the zooplankton community constitutes a network of

483   diverse taxa that is not as efficient at using the low amount of material fluxing. Our results are

484   consistent with previous studies suggesting that those oligotrophic regimes can be relatively

485   efficient at exporting the slow-sinking fraction of the little carbon that is produced in the surface

486   layers due to a low impact of zooplankton grazing on the sinking particles (Guidi et al., 2009;

487   Henson et al., 2015). This could help explain why we found the lowest particle flux attenuation

488   rates in the tropics.

489   **Global vertical patterns of zooplankton and particle flux**

490   The concentration and biomass of various zooplankton groups decreased with depth

491   (Fig. S1), confirming the general trend of decreasing zooplankton abundance and biomass from

492   the surface to 1000 m depth resolved (Fig. 2; Bode et al., 2018; Brugnano et al., 2012;

493   Hernández-León et al., 2020; Koppelmann et al., 2005; Kosobokova and Hopcroft, 2010;

494   Yamaguchi et al., 2004). Among these earlier studies, two models for the attenuation of

495   zooplankton have been proposed: an exponential or a power model. Here, we used the power

496   model (equation 1) because it was widely used to model vertical flux attenuation rates (Martin

497   et al., 1987). Based on this power model, we observed rates of decrease in zooplankton

498   abundance or biomass (Fig. 3) that were in the same range as those reported in the western

499   Pacific Ocean (-1.52 to -1.41 for abundance and -1.32 to -1.10 for biomass, (Yamaguchi et al.,

500   2002). Zooplankton abundance decreased more rapidly with depth than biomass as the average

501   size of organisms increased with depth, confirming that the contribution of larger species

502   increases with depth (Homma and Yamaguchi, 2010; Yamaguchi et al., 2002). Considering a

503   larger latitudinal band than earlier studies who found weak regional or global patterns

504   (Hernández-León et al., 2020; Puelles et al., 2019), we showed that the rates of zooplankton

505   attenuation vary with latitude and to a lesser extent with oxygen concentrations (Fig. 3) and

506   also in the opposite direction of the flux attenuation.

507   Stronger surface particle fluxes and vertical attenuation rates were found at higher

508   latitudes where primary production is mainly ensured by the microphytoplankton and weaker

509   flux and attenuation was found in the low latitude dominated by picophytoplankton (Fig.4).

510   Such latitudinal pattern in particle attenuation rates results from the gradient in the production

511   regime and has been observed quasi-systematically with imaging systems on global scales

512   (Guidi et al., 2015), but also based on sediment traps (Berelson, 2001) or combining sediment

513   traps with satellite-based estimates of primary production (Henson et al., 2012). However,

514   several short-term experiments at selected sites from temperate to tropical latitudes of the

515   Pacific and Atlantic, showed an opposite pattern with stronger flux and attenuation in cold and

516   productive regions compared to inter-tropical oligotrophic (Buesseler et al., 2007; Marsay et

517   al., 2015). The inconsistency of the observations is difficult to explain although it was noted

518   that depth varying remineralisation due to varying temperature may reconcile the contrasted

519   results (Marsay et al., 2015). It is possible that some of the differences arise from the use of

520   different methodologies (instruments, time scale, global representation of the dataset) to address

521   the complexity of the processes to be measured simultaneously.

522   Such opposite pattern between A_Zoo and B_zoo in one hand and A_Flux in the other

523   hand supports the view that the abundant zooplankton community plays a crucial role in flux

524   attenuation in productive layers, by feeding and fragmenting the sinking material as suggested

525   in previous studies (Dilling and Alldredge, 2000; Lampitt et al., 1990; Sarah L. C. Giering et

526   al., 2014; Stemmann et al., 2004). However, on average and more importantly at high latitudes,

527   zooplankton attenuation rates were stronger than the vertical flux attenuation rates (Fig. 3)

528   indicating that zooplankton vertical zonation may be affected by other processes than the

529   resources provided by the flux of organic matter from the epipelagic layer. In the inter-tropical

530   OMZ regions, zooplankton vertical attenuation rates were maximum when the vertical

531   attenuation of the particle's flux was minimum. Previous studies have reported lower flux

532   attenuation rates in the OMZ of the Arabian Sea (Haake et al., 1992; Roullier et al., 2014), and

533   Eastern Tropical North Pacific (Cavan et al., 2017; Van Mooy et al., 2002). Lower zooplankton

534   activity together with reduced bacterial activity (Cram et al., 2021) would allow sinking

535   particles to transit through the OMZ core without being severely degraded (Wishner et al., 2008,

536   1995) .

537

Sensitivity of plankton and vertical flux to contrasted oxygen conditions

539   By comparing zooplankton communities from inter-tropical stations with those from

540   oxygenated mesopelagic layers to stations from OMZs, our analysis brought additional

541   evidence that change in zooplankton community composition may affect the efficiency of the

542   BCP. The zooplankton community sampled in the Indian Ocean OMZ displayed a particular

543   composition compared to the other samples, which is in line with the increasing number of

544   studies that document the profound impact of oxygen depletion on pelagic organisms (Ekau et

545   al., 2010; Hauss et al., 2016; Wishner et al., 2018). Our results underlined how the OMZ can

546   strongly reduce the abundance of several zooplankton groups (i.e. Calanoida, Euphausiacea,

547   Amphipoda, Ostracoda) that are outcompeted by more hypoxia-tolerant ones. We found that

548   tunicates (mostly Appendicularia), large protists (Collodaria and Foraminifera), polychaetes,

549   Oncaeidae, Oithinidae and to a lesser extent Cnidaria (jellyfishes) may tolerate OMZ

550   conditions, since their abundance at OMZ and at non-OMZ stations did not present significant

551   differences. All of these zooplankton groups have been reported as being able to thrive or

552   endure at low oxygen concentrations in various OMZs (Ekau et al., 2010; Hauss et al., 2016;

553   Keister and Tuttle, 2013; Kiko and Hauss, 2019; Parris et al., 2014; Tutasi and Escribano, 2020;

554   Werner and Buchholz, 2013; Wishner et al., 2020). Those "hypoxiphilic" or hypoxia-tolerant

555   taxa display special adaptations that enable them to remain at extremely low oxygen

556   concentrations where other zooplankton groups cannot, because they fail to meet their

557   metabolic oxygen demand (Childress and Seibel, 1998; Seibel, 2011). Jellyfish and large

558   protists benefit from their passive feeding tactics which are less oxygen-demanding than active

559   cruising and filter feeding (Kiørboe, 2011). Indeed, hypoxia-tolerant taxa can also display

560   behavioral adaptations that cut down the metabolic costs associated with active feeding or the

561   active search for mates in the water column. Copepod species belonging to the Oncaeidae and

562   Oithonidae families are known for performing ambush feeding tactics or to attach themselves

563   on large detritus (Brun et al., 2017), which allows them to capture small preys or to feed on

564   falling detritus at very low metabolic costs. Therefore, these less motile copepods frequently

565   outcompete most of their calanoid congeners in OMZs and often co-occur with Appendicularia,

566   as those discard particle-rich aggregates on which the copepods feed (Alldredge, 1972; Brun et

567   al., 2017; Kiørboe, 2011). Other possible adaptations consist in the use of lipid storages and

568   metabolic suppression(Wishner et al., 2020). Some organisms conduct a diapause in the OMZ

569   for an extended period, allowing them to avoid foraging predators and to complete their life

570   cycle (Arashkevich et al., 1996). Diapause reduces energetic costs and thus allows the

571   organisms to survive in resource-depleted conditions. Metabolic suppression goes hand in hand

572   with the diapause, but can also occur on shorter time scales, e.g. when organisms stay at OMZ

573   depth during diel vertical migrations. Diapause and metabolic suppression are associated with

574   reduced respiratory and locomotor activity. Feeding on and disruption of particles could

575   therefore be reduced at OMZ depth not only due to the exclusion of many hypoxia intolerant

576   zooplankton organisms, but also due to the reduced activity of those zooplankton organisms

577   that can cope with OMZ conditions. The zooplankton groups we found to characterize the

578   community inhabiting the hypoxic and anoxic layers are those that commonly outcompete

579   others in OMZs worldwide. They could benefit from the likely future expansion of OMZ

580   (Oschlies et al., 2018) and thus become increasingly abundant with future climate change. This

581   would probably result in enhanced vertical particle flux in those regions. However, this requires

582   further research as some of these organisms could already be living near their physiological

583   hypoxia tolerance limits (Wishner et al., 2018).

Conclusions

584

585   Our study combined consistent and large-scale observations of zooplankton abundance,

586 biomass and community composition with estimates of vertical particle fluxes obtained through

587 imaging system pipelines. We showed that consistent observations can be obtained at a global

588 level using in situ camera systems and precise net sampling in various ecosystems

589 representative of different ocean conditions. In future surveys, consistently combining these

590 techniques with acoustic and other bio-optical sensors will allow the measurement of the

591 vertical and horizontal distribution of organisms with greater precision. We showed that the key

592 environmental variables driving epipelagic mesozooplankton community structure at the global

593 scale are temperature, phytoplankton biomass and phytoplankton key groups. In the

594 mesopelagic layer, surface phytoplankton size classes, particle concentration, temperature and

595 oxygen availability were identified as the main drivers of mesozooplankton community

596 structure. Our work furthermore suggests that low attenuation of zooplankton abundance and

597 biomass go in hand with high particle flux attenuation and vice versa.Such information is

598 crucial for the parameterization of the next generation of marine ecosystem models that describe

599 complex zooplankton-related processes based on coarse but increasingly numerous functional

600 types. Such models suggest that surface phytoplankton biomass and size classes, the flux of

601 particles and the oxygen content in the mesopelagic layer will all be affected further by global

602 climate change. The fact that zooplankton communities are sensitive to those factors suggests

603 that future climatic changes may profoundly alter zooplankton communities worldwide, at the

604 surface but also in the deeper mesopelagic layer.

605

632

References

Alldredge, A.L., 1972. Abandoned larvacean houses : a unique food source in pelagic environment. Science 177, 885.

Andersen, V., Francois, F., Sardou, J., Picheral, M., Scotto, M., Nival, P., 1998. Vertical distributions of macroplankton and micronekton in the Ligurian and Tyrrhenian Seas (northwestern Mediterranean). Oceanologica Acta 21, 655–676.

Arashkevich, E., Drits, A., Timonin, A., 1996. Diapause in the life cycle of Calanoides carinatus (Kroyer),(Copepoda, Calanoida). Hydrobiologia 320, 197–208.

Balazy, K., Trudnowska, E., Wichorowski, M., Błachowiak-Samołyk, K., 2018. Large versus small zooplankton in relation to temperature in the Arctic shelf region. Polar Research 37, 1427409.

Banse, K., 1964. On the vertical distribution of zooplankton in the sea. Progress in oceanography 2, 53–125.

Beaugrand, G., Conversi, A., Atkinson, A., Cloern, J., Chiba, S., Fonda-Umani, S., Kirby, R.R., Greene, C.H., Goberville, E., Otto, S.A., Reid, P.C., Stemmann, L., Edwards, M., 2019. Prediction of unprecedented biological shifts in the global ocean. Nature Climate Change 9, 237-+. https://doi.org/10.1038/s41558-019-0420-1

Berelson, W.M., 2002. Particle settling rates increase with depth in the ocean. Deep-Sea Research Part Ii-Topical Studies in Oceanography 49, 237–251.

Berelson, W.M., 2001. The Flux of Particulate Organic Carbon Into the Ocean Interior: A Comparison of Four U.S. JGOFS Regional Studies. Oceanography 14, 59–67.

Biard, T., Stemmann, L., Picheral, M., Mayot, N., Vandromme, P., Hauss, H., Gorsky, G., Guidi, L., Kiko, R., Not, F., 2016. In situ imaging reveals the biomass of giant protists in the global ocean. Nature 532, 504-+. https://doi.org/10.1038/nature17652

Bode, M., Hagen, W., Cornils, A., Kaiser, P., Auel, H., 2018. Copepod distribution and biodiversity patterns from the surface to the deep sea along a latitudinal transect in the eastern Atlantic Ocean (24°N to 21°S). Progress in Oceanography 161, 66–77. https://doi.org/10.1016/j.pocean.2018.01.010

Böttger-Schnack, R., 1996. Vertical structure of small metazoan plankton, especially noncalanoid copepods. I. Deep Arabian Sea. Journal of Plankton Research 18, 1073–1101. https://doi.org/10.1093/plankt/18.7.1073

Brugnano, C., Granata, A., Guglielmo, L., Zagami, G., 2012. Spring diel vertical distribution of copepod abundances and diversity in the open Central Tyrrhenian Sea (Western Mediterranean). Journal of Marine Systems 105, 207–220.

Brun, P., Payne, M.R., Kiørboe, T., 2017. A trait database for marine copepods. Earth System Science Data 9, 99–113.

Buesseler, K.O., Lamborg, C.H., Boyd, P.W., Lam, P.J., Trull, T.W., Bidigare, R.R., Bishop, J.K.B., Casciotti, K.L., Dehairs, F., Elskens, M., Honda, M., Karl, D.M., Siegel, D.A., Silver, M.W., Steinberg, D.K., Valdes, J., Van Mooy, B., Wilson, S., 2007. Revisiting Carbon Flux Through the Ocean's Twilight Zone. Science 316, 567–570. https://doi.org/10.1126/science.1137959

Cavan, E.L., Henson, S.A., Belcher, A., Sanders, R., 2017. Role of zooplankton in determining the efficiency of the biological carbon pump. Biogeosciences 14, 177–186.

Childress, J.J., Seibel, B.A., 1998. Life at stable low oxygen levels: adaptations of animals to oceanic oxygen minimum layers. The Journal of experimental biology 201, 1223–1232.

Chust, G., Allen, J.I., Bopp, L., Schrum, C., Holt, J., Tsiaras, K., Zavatarelli, M., Chifflet, M., Cannaby, H., Dadou, I., 2014. Biomass changes and trophic amplification of

683   plankton in a warmer ocean. Global Change Biology 20, 2124–2139.

684   Coma, R., Ribes, M., Serrano, E., Jiménez, E., Salat, J., Pascual, J., 2009. Global
685   warming-enhanced stratification and mass mortality events in the Mediterranean.
686   Proceedings of the National Academy of Sciences 106, 6176–6181.

687   Cram, J., Fuchsman, C., Duffy, M., Pretty, J., Lekanoff, R., Neibauer, J., Leung, S.,
688   Huebert, K.B., Weber, T., Bianchi, D., 2021. Slow particle remineralization, rather
689   than suppressed disaggregation, drives efficient flux transfer through the Eastern
690   Tropical North Pacific Oxygen Deficient Zone. Earth and Space Science Open Archive
691   ESSOAr.

692   Dilling, L., Alldredge, A.L., 2000. Fragmentation of marine snow by swimming
693   macrozooplankton: A new process impacting carbon cycling in the sea. Deep-Sea
694   Research Part I-Oceanographic Research Papers 47, 1227–1245.

695   Ekau, W., Auel, H., Portner, H.O., Gilbert, D., 2010. Impacts of hypoxia on the structure
696   and processes in pelagic communities (zooplankton, macro-invertebrates and fish).
697   Biogeosciences 7, 1669–1699. https://doi.org/10.5194/bg-7-1669-2010

698   Everett, J.D., Baird, M.E., Buchanan, P., Bulman, C., Davies, C., Downie, R., Griffiths,
699   C., Heneghan, R., Kloser, R.J., Laiolo, L., 2017. Modeling what we sample and
700   sampling what we model: challenges for zooplankton model assessment. Frontiers in
701   Marine Science 4, 77.

702   Fernández de Puelles, M., Gazá, M., Cabanellas-Reboredo, M., Santandreu, M., Irigoien,
703   X., González-Gordillo, J.I., Duarte, C.M., Hernández-León, S., 2019. Zooplankton
704   abundance and diversity in the tropical and subtropical ocean. Diversity 11, 203.

705   Forest, A., Babin, M., Stemmann, L., Picheral, M., Sampei, M., Fortier, L., Gratton, Y.,
706   Belanger, S., Devred, E., Sahlin, J., Doxaran, D., Joux, F., Ortega-Retuerta, E., Martin,
707   J., Jeffrey, W.H., Gasser, B., Miquel, J.C., 2013. Ecosystem function and particle flux
708   dynamics across the Mackenzie Shelf (Beaufort Sea, Arctic Ocean): an integrative
709   analysis of spatial variability and biophysical forcings. Biogeosciences 10, 2833–
710   2866. https://doi.org/10.5194/bg-10-2833-2013

711   Gaard, E., Gislason, A., Falkenhaug, T., Søiland, H., Musaeva, E., Vereshchaka, A.,
712   Vinogradov, G., 2008. Horizontal and vertical copepod distribution and abundance on
713   the Mid-Atlantic Ridge in June 2004. Deep Sea Research Part II: topical studies in
714   oceanography 55, 59–71.

715   Gallienne, C.P., Robins, D.B., Woodd-Walker, R.S., 2001. Abundance, distribution and
716   size structure of zooplankton along a 20 degrees west meridional transect of the
717   northeast Atlantic Ocean in July. Deep-Sea Research Part Ii-Topical Studies in
718   Oceanography 48, 925–949.

719   Gehlen, M., Bopp, L., Ernprin, N., Aumont, O., Heinze, C., Raguencau, O., 2006.
720   Reconciling surface ocean productivity, export fluxes and sediment composition in a
721   global biogeochemical ocean model. Biogeosciences 3, 521–537.

722   Guidi, L., Chaffron, S., Bittner, L., Eveillard, D., Larhlimi, A., Roux, S., Darzi, Y., Audic,
723   S., Berline, L., Brum, J.R., Coelho, L.P., Espinoza, J.C.I., Malviya, S., Sunagawa, S.,
724   Dimier, C., Kandels-Lewis, S., Picheral, M., Poulain, J., Searson, S., Stemmann, L.,
725   Not, F., Hingamp, P., Speich, S., Follows, M., Karp-Boss, L., Boss, E., Ogata, H.,
726   Pesant, S., Weissenbach, J., Wincker, P., Acinas, S.G., Bork, P., de Vargas, C.,
727   Iudicone, D., Sullivan, M.B., Raes, J., Karsenti, E., Bowler, C., Gorsky, G., Tara
728   Oceans Consortium Coordinator, 2016. Plankton networks driving carbon export in
729   the oligotrophic ocean. Nature 532, 465-+.

730   Guidi, L., Jackson, G.A., Stemmann, L., Miquel, J.C., Picheral, M., Gorsky, G., 2008.
731   Relationship between particle size distribution and flux in the mesopelagic zone.
732   Deep-Sea Research Part I-Oceanographic Research Papers 55, 1364–1374.

Guidi, L., Legendre, L., Reygondeau, G., Uitz, J., Stemmann, L., Henson, S.A., 2015. A new look at ocean carbon remineralization for estimating deepwater sequestration. Global Biogeochem. Cycles 29, 1044–1059. https://doi.org/10.1002/2014gb005063

Guidi, L., Stemmann, L., Jackson, G.A., Ibanez, F., Claustre, H., Legendre, L., Picheral, M., Gorsky, G., 2009. Effects of phytoplankton community on production, size and export of large aggregates: A world-ocean analysis. Limnology and Oceanography 54, 1951–1963. https://doi.org/10.4319/lo.2009.54.6.1951

Haake, B., Ittekkot, V., Ramaswamy, V., Nair, R., Honjo, S., 1992. Fluxes of amino acids and hexosamines to the deep Arabian Sea. Marine Chemistry 40, 291–314.

Hauss, H., Christiansen, S., Schütte, F., Kiko, R., Edvam Lima, M., Rodrigues, E., Karstensen, J., Löscher, C.R., Körtzinger, A., Fiedler, B., 2016. Dead zone or oasis in the open ocean? Zooplankton distribution and migration in low-oxygen modewater eddies. Biogeosciences 13, 1977–1989.

Henson, S.A., Sanders, R., Madsen, E., 2012. Global patterns in efficiency of particulate organic carbon export and transfer to the deep ocean. Global Biogeochemical Cycles 26.

Henson, S.A., Yool, A., Sanders, R., 2015. Variability in efficiency of particulate organic carbon export: A model study. Global Biogeochemical Cycles 29, 33–45.

Hernández-León, S., Koppelmann, R., Fraile-Nuez, E., Bode, A., Mompeán, C., Irigoien, X., Olivar, M.P., Echevarría, F., de Puelles, M.F., González-Gordillo, J.I., 2020. Large deep-sea zooplankton biomass mirrors primary production in the global ocean. Nature communications 11, 1–8.

Hidalgo, P., Escribano, R., Fuentes, M., Jorquera, E., Vergara, O., 2012. How coastal upwelling influences spatial patterns of size-structured diversity of copepods off central-southern Chile (summer 2009). Progress in Oceanography 92, 134–145.

Hirche, H.-J., Mumm, N., 1992. Distribution of dominant copepods in the Nansen Basin, Arctic Ocean, in summer. Deep Sea Research Part A. Oceanographic Research Papers 39, S485–S505.

Homma, T., Yamaguchi, A., 2010. Vertical changes in abundance, biomass and community structure of copepods down to 3000 m in the southern Bering Sea. Deep Sea Research Part I: Oceanographic Research Papers 57, 965–977.

Ibarbalz, F.M., Henry, N., Brandao, M.C., Martini, V., Busseni, G., Byrne, H., Coelho, L.P., Endo, H., Gasol, J.M., Gregory, A.C., Mahe, F., Rigonato, J., Royo-Llonch, M., Salazar, G., Sanz-Saez, I., Scalco, E., Soviadan, D., Zayed, A.A., Zingone, A., Labadie, K., Ferland, J., Marec, C., Kandels, S., Picheral, M., Dimier, C., Poulain, J., Pisarev, S., Carmichael, M., Pesant, S., Acinas, S.G., Babin, M., Bork, P., Boss, E., Bowler, C., Cochrane, G., de Vargas, C., Follows, M., Gorsky, G., Grimsley, N., Guidi, L., Hingamp, P., Iudicone, D., Jaillon, O., Kandels, S., Karp-Boss, L., Karsenti, E., Not, F., Ogata, H., Pesant, S., Poulton, N., Raes, J., Sardet, C., Speich, S., Stemmann, L., Sullivan, M.B., Sunagawa, S., Wincker, P., Bopp, L., Lombard, F., Zinger, L., Tara Oceans, C., 2019. Global Trends in Marine Plankton Diversity across Kingdoms of Life. Cell 179, 1084-+. https://doi.org/10.1016/j.cell.2019.10.008

Irigoien, X., Klevjer, T.A., Røstad, A., Martinez, U., Boyra, G., Acuña, J.L., Bode, A., Echevarria, F., Gonzalez-Gordillo, J.I., Hernandez-Leon, S., 2014. Large mesopelagic fishes biomass and trophic efficiency in the open ocean. Nature communications 5, 1–10.

Iversen, M.H., Lampitt, R.S., 2020. Size does not matter after all: no evidence for a size-sinking relationship for marine snow. Progress in Oceanography 189, 102445.

Karsenti, E., Acinas, S.G., Bork, P., Bowler, C., De Vargas, C., Raes, J., Sullivan, M., Arendt, D., Benzoni, F., Claverie, J.M., Follows, M., Gorsky, G., Hingamp, P.,

783   Iudicone, D., Jaillon, O., Kandels-Lewis, S., Krzic, U., Not, F., Ogata, H., Pesant, S.,
784   Reynaud, E.G., Sardet, C., Sieracki, M.E., Speich, S., Velayoudon, D., Weissenbach,
785   J., Wincker, P., Tara Oceans, C., 2011. A Holistic Approach to Marine Eco-Systems
786   Biology. Plos Biology 9. https://doi.org/e1001177 10.1371/journal.pbio.1001177

787 Keister, J.E., Tuttle, L.B., 2013. Effects of bottom-layer hypoxia on spatial distributions
788   and community structure of mesozooplankton in a sub-estuary of Puget Sound,
789   Washington, USA. Limnology and Oceanography 58, 667–680.

790 Kiko, R., Biastoch, A., Brandt, P., Cravatte, S., Hauss, H., Hummels, R., Kriest, I., Marin,
791   F., McDonnell, A.M.P., Oschlies, A., Picheral, M., Schwarzkopf, F.U., Thurnherr,
792   A.M., Stemmann, L., 2017. Biological and physical influences on marine snowfall at
793   the equator. Nature Geoscience 10, 852-+. https://doi.org/10.1038/ngeo3042

794 Kiko, R., Brandt, P., Christiansen, S., Faustmann, J., Kriest, I., Rodrigues, E., Schütte, F.,
795   Hauss, H., 2020. Zooplankton-mediated fluxes in the eastern tropical North Atlantic.
796   Frontiers in Marine Science 1.

797 Kiko, R., Hauss, H., 2019. On the estimation of zooplankton-mediated active fluxes in
798   oxygen minimum zone regions. Frontiers in Marine Science 6, 741.

799 Kiørboe, T., 2013. Zooplankton body composition. Limnology and Oceanography 58,
800   1843–1850.

801 Kiørboe, T., 2011. What makes pelagic copepods so successful? Journal of Plankton
802   Research 33, 677–685.

803 Kiørboe, T., Visser, A., Andersen, K.H., Handling editor: Howard Browman, 2018. A
804   trait-based approach to ocean ecology. ICES Journal of Marine Science.
805   https://doi.org/10.1093/icesjms/fsy090

806 Koppelmann, R., Weikert, H., Halsband-Lenk, C., Jennerjahn, T., 2004.
807   Mesozooplankton community respiration and its relation to particle flux in the
808   oligotrophic eastern Mediterranean. Global Biogeochemical Cycles 18.

809 Koppelmann, R., Zimmermann-Timm, H., Weikert, H., 2005. Bacterial and zooplankton
810   distribution in deep waters of the Arabian Sea. Deep-Sea Research Part I-
811   Oceanographic Research Papers 52, 2184–2192.
812   https://doi.org/10.1016/j.dsr.2005.06.012

813 Kosobokova, K.N., Hopcroft, R.R., 2010. Diversity and vertical distribution of
814   mesozooplankton in the Arctic's Canada Basin. Deep Sea Research Part II: Topical
815   Studies in Oceanography 57, 96–110.

816 Kwiatkowski, L., Aumont, O., Bopp, L., 2019. Consistent trophic amplification of marine
817   biomass declines under climate change. Global change biology 25, 218–229.

818 Lampitt, R.S., Noji, T., Von Bodungen, B., 1990. What happens to zooplankton fecal
819   pellets ? Implication for material flux. Marine Biology 104, 15–23.

820 Laws, R.M., 1985. The ecology of the Southern Ocean. Amer. Scient. 73, 26–40.

821 Legendre, P., Legendre, L., 1998. Numerical ecology, 2nd english. ed, Developments in
822   environmental modelling 20. Elsevier, Amsterdam.

823 Lehette, P., Hernandez-Leon, S., 2009. Zooplankton biomass estimation from digitized
824   images: a comparison between subtropical and Antarctic organisms. Limnology and
825   Oceanography-Methods 7, 304–308.

826 Madhupratap, M., Nair, KNV, Venugopal, P., Gauns, M., Haridas, P., Gopalakrishnan,
827   T., Nair, KKC, 2004. Arabian Sea oceanography and fisheries.

828 Marsay, C.M., Sanders, R.J., Henson, S.A., Pabortsava, K., Achterberg, E.P., Lampitt,
829   R.S., 2015. Attenuation of sinking particulate organic carbon flux through the
830   mesopelagic ocean. Proceedings of the National Academy of Sciences 112, 1089–
831   1094.

832 Martin, J.H., Knauer, G.A., Karl, D.M., Broenkow, W.W., 1987. VERTEX: Carbon

833   cycling in the Northeast Pacific. Deep-Sea Research 34, 267–285.

834   Morrison, J.M., Codispoti, L., Smith, S.L., Wishner, K., Flagg, C., Gardner, W.D.,
835   Gaurin, S., Naqvi, S., Manghnani, V., Prosperie, L., 1999. The oxygen minimum zone
836   in the Arabian Sea during 1995. Deep Sea Research Part II: Topical Studies in
837   Oceanography 46, 1903–1931.

838   MOTODA, S., 1959. Devices of simple plankton apparatus. Memoirs of the faculty of
839   fisheries Hokkaido University 7, 73–94.

840   Ohman, M.D., Romagnan, J.B., 2016. Nonlinear effects of body size and optical
841   attenuation on Diel Vertical Migration by zooplankton. Limnology and Oceanography
842   61, 765–770. https://doi.org/10.1002/lno.10251

843   Oschlies, A., Brandt, P., Stramma, L., Schmidtko, S., 2018. Drivers and mechanisms of
844   ocean deoxygenation. Nature Geoscience 11, 467–473.

845   Paffenhofer, G.A., Mazzocchi, M.G., 2003. Vertical distribution of subtropical
846   epiplanktonic copepods. Journal of Plankton Research 25, 1139–1156.

847   Palomares-García, R.J., Gómez-Gutiérrez, J., Robinson, C.J., 2013. Winter and summer
848   vertical distribution of epipelagic copepods in the Gulf of California. Journal of
849   Plankton Research 35, 1009–1026.

850   Park, C., Wormuth, J., 1993. Distribution of Antarctic zooplankton around Elephant
851   Island during the austral summers of 1988, 1989, and 1990. Polar Biology 13, 215–
852   225.

853   Parris, D.J., Ganesh, S., Edgcomb, V.P., DeLong, E.F., Stewart, F.J., 2014. Microbial
854   eukaryote diversity in the marine oxygen minimum zone off northern Chile. Frontiers
855   in microbiology 5, 543.

856   Pesant, S., Not, F., Picheral, M., Kandels-Lewis, S., Le Bescot, N., Gorsky, G., Iudicone,
857   D., Karsenti, E., Speich, S., Trouble, R., Dimier, C., Searson, S., Tara Oceans
858   Consortium, C., 2015. Open science resources for the discovery and analysis of Tara
859   Oceans data. Scientific data 2, 150023–150023. https://doi.org/10.1038/sdata.2015.23

860   Quetin, L.B., Ross, R.M., Frazer, T.K., Haberman, K.L., 1996. Factors affecting
861   distribution and abundance of zooplankton, with an emphasis on Antarctic krill,
862   Euphausia superba. Antarctic Research Series 70, 357–371.

863   Remsen, A., Hopkins, T.L., Samson, S., 2004. What you see is not what you catch: a
864   comparison of concurrently collected net, Optical Plankton Counter, and Shadowed
865   Image Particle Profiling Evaluation Recorder data from the northeast Gulf of Mexico.
866   Deep-Sea Research Part I-Oceanographic Research Papers 51, 129–151.

867   Richardson, A.J., 2008. In hot water: zooplankton and climate change. ICES Journal of
868   Marine Science 65, 279–295. https://doi.org/10.1093/icesjms/fsn028

869   Robinson, C., Steinberg, D.K., Anderson, T.R., Aristegui, J., Carlson, C.A., Frost, J.R.,
870   Ghiglione, J.F., Hernandez-Leon, S., Jackson, G.A., Koppelmann, R., Queguiner, B.,
871   Ragueneau, O., Rassoulzadegan, F., Robison, B.H., Tamburini, C., Tanaka, T.,
872   Wishner, K.F., Zhang, J., 2010. Mesopelagic zone ecology and biogeochemistry - a
873   synthesis. Deep-Sea Research Part Ii-Topical Studies in Oceanography 57, 1504–
874   1518. https://doi.org/10.1016/j.dsr2.2010.02.018

875   Roe, H., 1988. Midwater biomass profiles over the Madeira Abyssal Plain and the
876   contribution of copepods, in: Biology of Copepods. Springer, pp. 169–181.

877   Rombouts, I., Beaugrand, G., Ibanez, F., Gasparini, S., Chiba, S., Legendre, L., 2010. A
878   multivariate approach to large-scale variation in marine planktonic copepod diversity
879   and its environmental correlates. Limnology and Oceanography 55, 2219–2229.
880   https://doi.org/10.4319/lo.2010.55.5.2219

881   Ross, R.M., Quetin, L.B., Martinson, D.G., Iannuzzi, R.A., Stammerjohn, S.E., Smith,
882   R.C., 2008. Palmer LTER: Patterns of distribution of five dominant zooplankton

883   species in the epipelagic zone west of the Antarctic Peninsula, 1993–2004. Deep Sea
884   Research Part II: Topical Studies in Oceanography 55, 2086–2105.
885 Roullier, F., Berline, L., Guidi, L., De Madron, X.D., Picheral, M., Sciandra, A., Pesant,
886   S., Stemmann, L., 2014. Particle size distribution and estimated carbon flux across the
887   Arabian Sea oxygen minimum zone. Biogeosciences 11, 4541–4557.
888   https://doi.org/10.5194/bg-11-4541-2014
889 Rutherford, S., D'Hondt, S., Prell, W., 1999. Environmental controls on the geographic
890   distribution of zooplankton diversity. Nature 400, 749–753.
891   https://doi.org/10.1038/23449
892 Saporiti, F., Bearhop, S., Vales, D.G., Silva, L., Zenteno, L., Tavares, M., Crespo, E.A.,
893   Cardona, L., 2015. Latitudinal changes in the structure of marine food webs in the
894   Southwestern Atlantic Ocean. Marine Ecology Progress Series 538, 23–34.
895 Sarah L. C. Giering, Richard Sanders, Richard S. Lampitt, Thomas R. Anderson,
896   Christian Tamburini, Mehdi Boutrif, Mikhail V. Zubkov, Chris M. Marsay, Stephanie
897   A. Henson, Kevin Saw, Kathryn Cook, Daniel J. Mayor, 2014. Reconciliation of the
898   carbon budget in the ocean's twilight zone. Nature 507, 17.
899   https://doi.org/10.1038/nature13123
900 Schmidtko, S., Stramma, L., Visbeck, M., 2017. Decline in global oceanic oxygen content
901   during the past five decades. Nature 542, 335–339.
902 Seibel, B.A., 2011. Critical oxygen levels and metabolic suppression in oceanic oxygen
903   minimum zones. Journal of Experimental Biology 214, 326–336.
904 Smith, S., Roman, M., Prusova, I., Wishner, K., Gowing, M., Codispoti, L.A., Barber, R.,
905   Marra, J., Flagg, C., 1998. Seasonal response of zooplankton to monsoonal reversals
906   in the Arabian Sea. Deep-Sea Research Part II 45, 2369–2403.
907 St John, M.A., Borja, A., Chust, G., Heath, M., Grigorov, I., Mariani, P., Martin, A.P.,
908   Santos, R.S., 2016. A dark hole in our understanding of marine ecosystems and their
909   services: perspectives from the mesopelagic community. Frontiers in Marine Science
910   3, 31.
911 Steinberg, D.K., Landry, M.R., 2017. Zooplankton and the ocean carbon cycle. Annual
912   review of marine science 9, 413–444.
913 Stemmann, L., Jackson, G.A., Gorsky, G., 2004. A vertical model of particle size
914   distributions and fluxes in the midwater column that includes biological and physical
915   processes - Part II: application to a three year survey in the NW Mediterranean Sea.
916   Deep-Sea Research Part I-Oceanographic Research Papers 51, 885–908.
917   https://doi.org/10.1016/j.dsr.2004.03.002
918 Stempniewicz, L., Błachowiak-Samołyk, K., Węsławski, J.M., 2007. Impact of climate
919   change on zooplankton communities, seabird populations and arctic terrestrial
920   ecosystem—a scenario. Deep Sea Research Part II: Topical Studies in Oceanography
921   54, 2934–2945.
922 Stramma, L., Schmidtko, S., Levin, L.A., Johnson, G.C., 2010. Ocean oxygen minima
923   expansions and their biological impacts. Deep Sea Research Part I: Oceanographic
924   Research Papers 57, 587–595. https://doi.org/10.1016/j.dsr.2010.01.005
925 Stukel, M.R., Ohman, M.D., Kelly, T.B., Biard, T., 2019. The roles of suspension-feeding
926   and flux-feeding zooplankton as gatekeepers of particle flux into the mesopelagic
927   ocean in the Northeast Pacific. Frontiers in Marine Science 6, 397.
928 Tarling, G.A., Shreeve, R.S., Ward, P., Atkinson, A., Hirst, A.G., 2004. Life-cycle
929   phenotypic composition and mortality of Calanoides acutus (Copepoda : Calanoida) in
930   the Scotia Sea: a modelling approach. Marine Ecology-Progress Series 272, 165–181.
931 Terazaki, M., Wada, M., 1988. Occurrence of large numbers of carcasses of the large,
932   grazing copepod Calanus cristatus from the Japan Sea. Marine Biology 97, 177–183.

933 Trudnowska, E., Lacour, L., Ardyna, M., Rogge, A., Irisson, J.O., Waite, A.M., Babin,
934   M., Stemmann, L., 2021. Marine snow morphology illuminates the evolution of
935   phytoplankton blooms and determines their subsequent vertical export. Nature
936   communications 12, 2816–2816. https://doi.org/10.1038/s41467-021-22994-4
937 Tutasi, P., Escribano, R., 2020. Zooplankton diel vertical migration and downward C flux
938   into the oxygen minimum zone in the highly productive upwelling region off northern
939   Chile. Biogeosciences 17, 455–473.
940 Uitz, J., Claustre, H., Morel, A., Hooker, S.B., 2006. Vertical distribution of
941   phytoplankton communities in open ocean: An assessment based on surface
942   chlorophyll. Journal of Geophysical Research. C. Oceans 111,
943   [doi:10.1029/2005JC003207].
944 Van Mooy, B.A., Keil, R.G., Devol, A.H., 2002. Impact of suboxia on sinking particulate
945   organic carbon: Enhanced carbon flux and preferential degradation of amino acids via
946   denitrification. Geochimica et Cosmochimica Acta 66, 457–465.
947 Vaquer-Sunyer, R., Duarte, C.M., 2008. Thresholds of hypoxia for marine biodiversity.
948   Proceedings of the National Academy of Sciences 105, 15452–15457.
949 Werner, T., Buchholz, F., 2013. Diel vertical migration behaviour in Euphausiids of the
950   northern Benguela current: seasonal adaptations to food availability and strong
951   gradients of temperature and oxygen. Journal of Plankton Research 35, 792–812.
952 Wheeler Jr, E., 1967. Copepod detritus in the deep sea. Limnology and Oceanography
953   12, 697–702.
954 Wishner, K.F., Ashjian, C.J., Gelfman, C., Gowing, M.M., Kann, L., Levin, L.A.,
955   Mullineaux, L.S., Saltzman, J., 1995. Pelagic and Benthic Ecology of the Lower
956   Interface of the Eastern Tropical Pacific Oxygen Minimum Zone. Deep Sea Res. 42,
957   93–115.
958 Wishner, K.F., Gelfman, C., Gowing, M.M., Outram, D.M., Rapien, M., Williams, R.L.,
959   2008. Vertical zonation and distributions of calanoid copepods through the lower
960   oxycline of the Arabian Sea oxygen minimum zone. Prog. Oceanogr. 78, 163–191.
961   https://doi.org/10.1016/j.pocean.2008.03.001
962 Wishner, K.F., Seibel, B., Outram, D., 2020. Ocean deoxygenation and copepods: coping
963   with oxygen minimum zone variability. Biogeosciences 17, 2315–2339.
964 Wishner, K.F., Seibel, B.A., Roman, C., Deutsch, C., Outram, D., Shaw, C.T., Birk, M.A.,
965   Mislan, K., Adams, T., Moore, D., 2018. Ocean deoxygenation and zooplankton: very
966   small oxygen differences matter. Science advances 4, eaau5180.
967 Yamaguchi, A., Watanabe, Y., Ishida, H., Harimoto, T., Furusawa, K., Suzuki, S.,
968   Ishizaka, J., Ikeda, T., Mac Takahashi, M., 2004. Latitudinal differences in the
969   planktonic biomass and community structure down to the greater depths in the western
970   North Pacific. Journal of Oceanography 60, 773–787.
971 Yamaguchi, A., Watanabe, Y., Ishida, H., Harimoto, T., Furusawa, K., Suzuki, S.,
972   Ishizaka, J., Ikeda, T., Takahashi, M., 2002. Community and trophic structures
973   ofpelagic copepods down to greater depths in the western subarctic Paci fic (WEST-
974   COSMIC). Deep Sea Research Part I 49, 1007–1025.
975 Yasuhara, M., Hunt, G., Dowsett, H.J., Robinson, M.M., Stoll, D.K., 2012. Latitudinal
976   species diversity gradient of marine zooplankton for the last three million years.
977   Ecology Letters 15, 1174–1179. https://doi.org/10.1111/j.1461-0248.2012.01828.x
978
979
980

981

982

983

984   Table 1: List of the 19 taxa kept for the RDA analysis.

Taxonomic groups	Sub groups
Protista	Protista includes unrecognized protista on the images
Annelida	Images of all Annelida
Chaetognatha	Images of all Chaetognatha
Tunicata	Images of all Gelatinous filter feeders
Cnidaria	Images of all gelatinous carnivores belonging to Cnidaria
Mollusca	Images of all Pteropoda
Cladocera	Images of all Small Cladocera
Eumalacostraca	Images of all Decapoda but those distinguish at detailed taxonomic level
Euphausiacea	Images of all Euphausiacea
Amphipoda	Images of all Amphipoda
Ostracoda	Images of all Ostracoda
Crustacean_larvae	Images of all crustacean larvae
Other_Copepoda	Images of all Copepoda but those distinguish at detailed taxonomic level
Calanoida	Images of all Calanoida but those distinguish at detailed taxonomic level
Oithonidae	Images of all Oithonidae
Corycaeidae	Images of all Corycaeidae
Oncaeidae	Images of all Oncaeidae
Metridinidae	Images of all Metridinidae
Calanidae	Images of all Calanidae

985

986   Table 2: Coefficient factors used for equation 1 and that were taken from observed allometric

987   relationships between body area and individual dry mass (Lehette et al., 2009). The conversion factors

988   to carbon are taken from Kiorboe 2013.

Zooplankton category	Biomass Exponent (b)	Biomass Multiplier (a)	DW to C
Copepods	1.59 ± 0.03	45.25	0.48
Chaetognaths	1.19 ± 0.13	23.45	0.367
Decapods	1.48 ± 0.05	49.58	0.419
Cnidaria	1.02 ± 0.38	43.17	0.132
Tunicata	1.24 ± 0.08	4.03	0.103
Pteropods	1.54 ± 0.03	43.38	0.289
Protists*		0.08 mgC mm-3	
Other (Annelids, Cladocera, Ostracoda)	1.54 ± 0.03	43.38	0.289

989 * for the protist we used a conversion factor between biovolume and biomass (Biard et al.,
990 2016)
991

992

993 Table 3: Summary of the main mesozooplankton groups global proportion of abundance and biomass:

Taxa Proportion(%)	Epipelagic		Upper Mesopelagic		Lower Mesopelagic	
	Abundance	Biomass	Abundance	Biomass	Abundance	Biomass
All copepoda	84.89	65	84.80	76.39	94.5	96.5
Chaetognatha	3.67	8.39	2.44	3.48	2.06	2.53
Crust decapoda	2.9	18.9	0.36	14.98	0.00	0.00
Cnidaria	0.7	0.96	0.19	0.24	0.00	0.00
Tunicata	0.5	0.02	0.08	0.001	0.1	0.00
Protista	1.5	0.5	0.97	0.19	0.9	0.09
Pteropoda	1.2	0.6	0.41	0.03	0.00	0.00
Other (annelids, cladocera, ostracoda)	4.2	3.09	10.05	3.23	2.38	0.87

994

995 Table 4: Summary of the vertical attenuation rate (b: median and IC: confidence Interval) of

996 mesozooplankton abundance and biomass and particle vertical flux (b: median value and IC: confidence

997 Interval).

	Zooplankton abundance $(Ind.\,m^{-3})$		Zooplankton biomass $(mgC.\,m^{-3})$		Particle vertical flux	
	b	IC (95%)	b	IC (95%)	b	IC (95%)
ANOXIA_TROPIC	-1.82	-2.13 - -1.13	-1.3	-2.9 - -0.75	-0.26	-0.77- -0.19
TROPIC	-1.39	-2.46 - -0.69	-1.04	-1.92 - -0.58	-0.42	-0.78- -0.21
TEMPERATE	-1.19	-1.56 - -0.64	-0.89	-1.26 - -0.57	-0.50	-0.84- -0.11
POLAR	-1.18	-1.71 - -0.96	-0.83	-1.41 - -0.74	-0.78	-4.51- -0.36

998

999 Table 5: Probability of H0, no difference between the groups (pairwise Kruskal-Wallis test) for total

1000 zooplankton and biomass depth attenuation rates and particle flux attenuation rate. * Significant

1001 differences.

Two by two comparisons		Abundance	Biomass	Flux
Tropic-Anoxia	Tropic	0.057	0.641	0.77
Tropic-Anoxia	Temperate	0.0018*	0.189	0.82
Tropic-Anoxia	Polar	0.01*	0.238	0.09
Tropic	Temperate	0.34	0.639	0.99
Tropic	Polar	0.51	0.685	0.28
Temperate	Polar	0.99	1	0.52

1002

Supplementary material

Availability of the dataset

Data sets for the environment are available at Pangea:

(https://doi.org/10.1594/PANGAEA.840721)

Tables for the RDA are available

For zooplankton: Metadata_Zooplankton_Article_RDA.xls

Zooplankton Pangea for the tables/ecotaxa for the vignettes

https://ecotaxa.obs-vlfr.fr/prj/714?taxo=56693&taxochild=N&ipp=100&zoom=100&sortby=&magenabled=0&popupenabled=0&statusfilter=&samples=&instrum=&sortorder=asc&dispfield=&projid=714&pageoffset=0

Quality of the dataset

The analysis reported here is the first to apply consistent imaging techniques in order to investigate particle flux, zooplankton community composition and biomass across the global ocean. To do so, our study relies on the combined use of the Underwater Video Profiler v5 (UVP5), a Multinet and the Zooscan imaging system. These results are the first combined global zooplankton and flux estimates and as such provide a baseline for future studies. Their quality needs to be discussed with regards to 1) flux assessment, 2) mesh selectivity, mass conversion and possible impact of dead zooplankton in the images, the capacity of the sampling design to capture or not 3) day night variability and 4) mesopelagic peaks of zooplankton.

Vertical particle mass fluxes (mg Dry Weight $m^{-2}d^{-1}$) were calculated from the particle size spectra (150 μm -1.5 mm) detected by the UVP5 following Guidi et al., (2008). Briefly, the procedure optimized two parameters in the flux equation by comparing UVP5 derived flux and a global sediment trap flux data set (Guidi et al., 2008). Depending on the ocean basin, regional algorithms with different sets of the two parameters have been proposed (Forest et al., 2013; Kiko et al., 2017) but the shape of the allometric relationships between particle size and flux is kept as a growing monotonic power relationship. Many studies have shown that this assumption is verified when comparing extremes size of particles but they all have also shown

1037   a high variability (Guidi et al., 2008; Iversen and Lampitt, 2020) which cannot be depicted
1038   without more information on the type of particles. In addition, we used the same parametrization
1039   for each depth layer although a few observational and modelling studies (Berelson, 2002;
1040   Gehlen et al., 2006) have proposed that the sinking speed may vary with depth. Finally, the
1041   fluxes are calculated considering all particles detected in situ by the UVP5. Because particles
1042   are so abundant in the size range presently considered for flux estimation (150μm to 1.5mm),
1043   the impact of zooplankton in the present flux estimates is low (Guidi et al., 2015; Kiko et al.,
1044   2020). We did not perform further sensitivity analyses as the aim of this study was not to
1045   quantify absolute carbon flux but to assess correlations with zooplankton and other
1046   environmental variables. In the future, better recognition of particles on images will possibly
1047   allow to calculate different particle speed for different ypes of aggregates as was proposed
1048   recently (Trudnowska et al., 2021).

1049   Zooplankton abundance estimates are sensitive to the mesh of the plankton net tow used
1050   (Gallienne et al., 2001). A mesh size of 300μm was selected for the Multinet as a good
1051   compromise to capture both mesozooplankton and macro-zooplankton. However, the small
1052   copepod families (Oithona, Oncaeidae, Clausocalanidae, Paracalanidae) that dominate
1053   community composition in tropical/subtropical open oceans are not collected in an optimal
1054   fashion with the present mesh size, contrary to the larger Calanidae notably in the temperate
1055   and polar regions. Therefore, our abundance estimates likely underestimate the contribution of
1056   the smallest mesozooplankton groups. Nonetheless, even a net equipped with a 150 μm mesh
1057   can still underestimate the abundance of cyclopoids and early copepod stages (Paffenhofer and
1058   Mazzocchi, 2003).

1059   Nets can also destroy fragile organisms during the sampling process (Remsen et al.,
1060   2004). For example, the very low abundance and biomass of Rhizarians reported here
1061   contrasting with recent findings based on *in situ* cameras (Biard et al., 2016). This is likely due
1062   to such sampling biases. As for the estimation of particle fluxes from particle size spectra, we
1063   assessed the carbon biomass of each individual organism's size using published allometric
1064   relationships (Lehette and Hernández-León, 2009) in which large and rare organisms
1065   contributes importantly to the total biomass bringing strong variability in the results. To account
1066   for the excessive variability in biomass estimates, we analysed our results using both abundance
1067   and biomass.

1068   Dead zooplankton, including carcasses, are increasingly recognized as being quite
1069   abundant in the mesopelagic water (Böttger-Schnack, 1996; Roe, 1988; Terazaki and Wada,
1070   1988; Wheeler Jr, 1967). It is impossible to assess whether the damages of the organisms

1071 observed on the digitized organisms were inflicted by the net tow. This is even harder to assess
1072 in the deeper nets which spent more time in the water column. Therefore, we cannot tell whether
1073 the organisms were damaged during the sampling process or dead beforehand. We attempted
1074 to separate the carcasses from the complete bodies of copepods based on grey intensity criteria
1075 or by looking at the physical integrity of the organisms, but this was not successful because of
1076 independent and continuous changes for both criteria. Nonetheless, among the 110'000
1077 vignettes of copepods, 21'117 (20%) were initially classified as possible carcasses. Their
1078 proportion was equal to 42.90% in the surface layer, 26.71% in the upper mesopelagic and
1079 30.39% in the deepest layers. The median and interquartile of abundances varied from the
1080 surface (median = 1.21 Ind/m^3, IQR = 2.53) to the upper mesopelagic (median = 0.75, IQR =
1081 0.89) and increased towards deeper layers (median = 0.85, IQR = 0.99). Subsequent data
1082 analyses showed that aggregating them or not with the non-damaged copepods had no effect on
1083 the analysis' results because their proportion was homogeneous across sampling sites.
1084 Therefore, all copepods were ultimately pooled together for all our numerical analyses.

1085   Zooplankton and micronekton perform diel vertical migration (DVM) in all oceans
1086 (Banse, 1964). Depending on the organism's taxonomic group and size, ranges of diel migration
1087 show tremendous variability (Ohman and Romagnan, 2016; Tarling et al., 2004) . In our study,
1088 significant differences in abundances between day and night samples was found for a few
1089 groups known to be diel migrators (Euphausiids, Metridinidae, Corycaeidae, Cnidaria for
1090 abundance data; and Eumalacostraca and Ostracoda for biomass data). However, at the
1091 community level (i.e., total mesozooplankton), no significant differences could be found
1092 between the day and night samples at surface. However, total zooplankton biomass was higher
1093 in night samples compared to day samples, because of the more abundant large-bodied
1094 migrators (Eumalacostraca, Euphausiacea, Table S2). For abundance, this is a rather
1095 unexpected result as a large number of zooplankton taxa perform DVM (Kiørboe et al., 2018;
1096 Ohman and Romagnan, 2016). Yet, this absence of significant changes had already been
1097 observed in previous studies using similar types of plankton nets (Wishner et al., 2018). DVM
1098 could not be detected from the ANOSIM analysis of the surface layer for different reasons.
1099 First, the weak diel differences in abundances could easily be smeared by plankton patchiness
1100 when the replicates are too low. Second, it is possible that no differences were observed because
1101 the large organisms carrying out DVM are too few in number compared to the smaller ones in
1102 the present data. Day and night differences between the slopes of the total biomass were found,
1103 probably due to the few diel migrators species. Hence, it is well known that large zooplankton
1104 (euphausiids, sergestid shrimps, amphipods, fish such as myctophids(Morrison et al., 1999))

1105   sampled with larger Multinet nets (opening $>1m^2$ and mesh size $>500\mu m$), or detected through

1106   acoustics techniques, showed stronger DVM than smaller organisms collected through smaller

1107   Multinet nets such as ours (opening of 0.25 m^2 and mesh size of $300\mu m$). Furthermore,

1108   copepods contributed to nearly 80% of total zooplankton abundance in our samples, and

1109   copepod DVM may be confined most typically to populations living within the epipelagic zone

1110   (Madhupratap et al., 2004; Morrison et al., 1999; Smith et al., 1998).

1111   Many studies have reported midwater peaks of zooplankton and nekton in 100-200 m

1112   depth layers centered around 40 to 600 m depth (Andersen et al., 1998; Irigoien et al., 2014;

1113   Koppelmann et al., 2004) indicating that the use of a simple power law to describe plankton

1114   biomass may be an oversimplification of the true vertical zonation. The general lack of such

1115   peaks may be explained by the variability in methods used between studies. Midwater peaks

1116   are often reported with instruments allowing a good vertical resolution (> 10 observations in

1117   the upper kilometer) and targeting the large migrating organisms with nets having large mesh

1118   size or acoustic devices with frequencies adapted to nektonic organisms. Many studies using

1119   Multinets equipped with rather fine mesh size ($<500\mu m$) do not capture such peaks in

1120   abundance/ biomass (Homma and Yamaguchi, 2010; Yamaguchi et al., 2002). In our study, the

1121   mesopelagic layer was sampled down to 900 m depth, and only with 2 or 3 nets with a mesh

1122   size of $300\mu m$ and a small net opening (0.25 m^2). Therefore, midwater peaks could have been

1123   smoothed in the few layers. Hence, the power law simplification may be a proper proxy for the

1124   smaller fraction of the mesozooplankton (mainly copepods smaller than 2 mm).

1125

1126

1127

Community vertical distribution

On a global scale, zooplankton average abundance and biomass decreased drasctically with depth, with quasi similar patterns for the eight main zooplankton groups (Fig. S1). The strongest variation in abundance was observed for copepods, followed by chaetognaths, small omnivorous zooplankton and crustacean decapods (Fig. S1). The strongest variation in biomass with depth were observed for copepods followed by decapods, chaetognaths and small omnivorous zooplankton (Fig. S2).
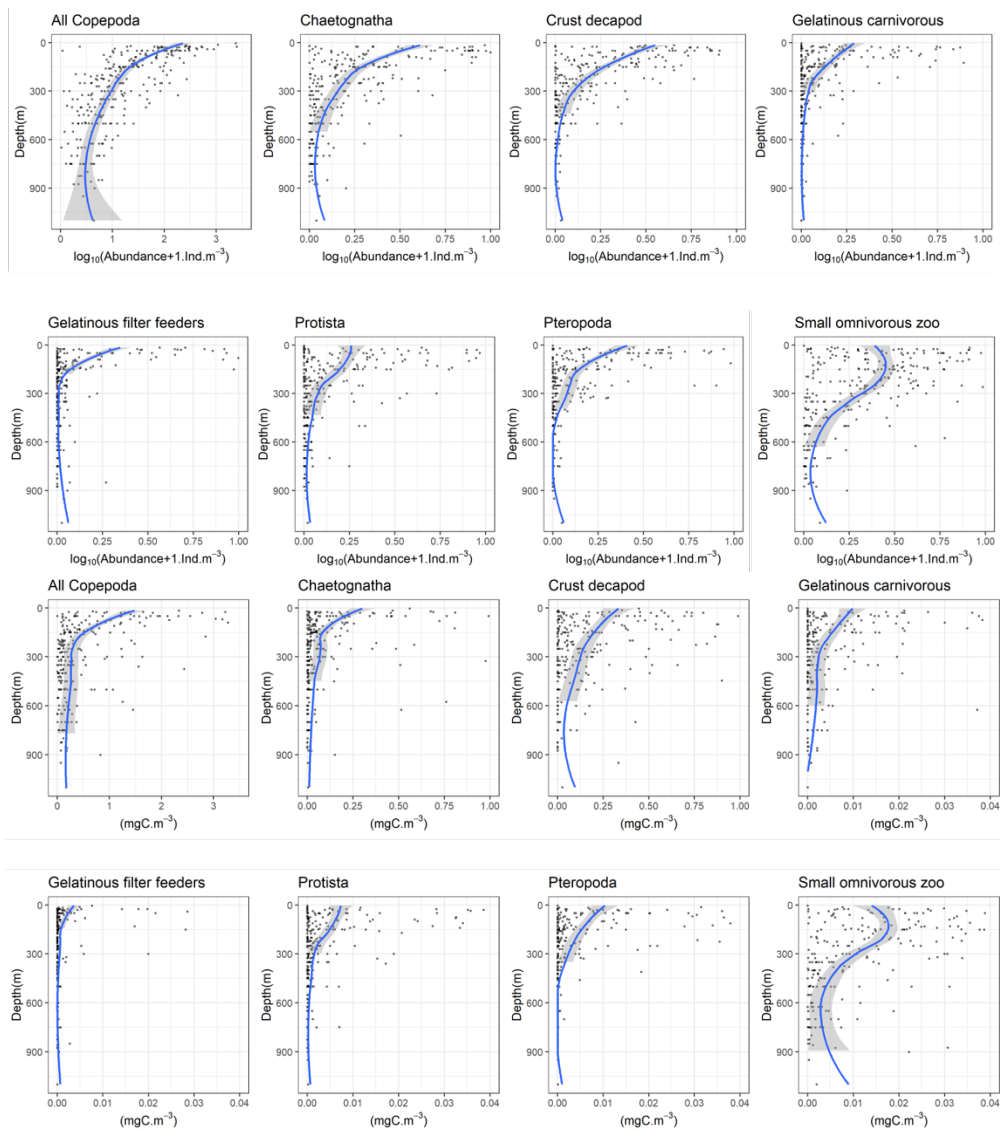
Fig. S1: Vertical profiles of abundance (two first lines) and biomass (two last lines) in the global ocean for the 8 functional mesozooplankton groups: all copepoda, chaetognatha, crustacean decapoda (crust decapod), gelatinous carnivorous, gelatinous filter feeders, protista, pteropoda, small omnivorous zooplankton. Not all abundance and biomass scales are similar to better observe the gradients. In all

1143 cases, solid lines correspond to a smooth trends and gray ribbons to the 95% confidence intervals. These

1144 trends are drawn for illustrative purposes and were not used in down- stream analyses.

1145

**Community composition in the upper first kilometer of the ocean**

1147   When analyzing all vertical layers together, the redundant discriminant analysis (RDA)

1148 indicated that environmental variables explained 27.01% of the variance in mesozooplankton

1149 groups abundance (Fig. 4). The first RDA axis (RDA1; 47.08% of the variance constrained by

1150 the RDA) opposed the samples from polar waters (Arctic Ocean, Southern Ocean; RDA1 > 0)

1151 to the samples taken at lower latitudes (Indian Ocean, Northern and Southern Atlantic Ocean,

1152 Northern and Southern Pacific Ocean; RDA1 < 0), especially for epipelagic and upper

1153 mesopelagic samples. RDA1 was negatively scored by variables depicting a gradient of tropical

1154 to extratropical conditions: temperature, salinity, and the relative contribution of

1155 picophytoplankton and nanophytoplankton to phytoplankton community biomass. Meanwhile,

1156 RDA1 was positively scored by dissolved oxygen concentration, the intensity of the vertical

1157 particle flux and its attenuation rate, the concentration of suspended particles and the

1158 contribution of microphytoplankton to total phytoplankton biomass. The second RDA axis

1159 (22.22 % of the constrained variance) opposed the samples from the surface (RDA2 < 0) to the

1160 samples from mesopelagic layers (RDA2 > 0). This axis was positively scored by depth,

1161 salinity, and nitrate concentrations, and negatively scored by pico-, nano- and

1162 microphytoplankton concentrations, oxygen concentration, particles and chlorophyll *a*

1163 concentrations. Samples from the epipelagic layer of higher latitudes showed higher plankton

1164 abundances and were dominated by Calanidae and crustacean larvae (copepod nauplii).

1165 Samples from the epipelagic layers of lower latitudes Tropical Ocean were more diverse as they

1166 displayed more even contributions of Protista, Eumalacostraca, Annelida, Amphipoda,

1167 Tunicata, Corycaeidae, Chaetognatha, Euphausiacea, Oithonidae, Cnidaria, Mollusca and

1168 Cladocera. In the mesopelagic layer, communities were less spread in the RDA space than for

1169 the surface layer. Mesopelagic communities were dominated by Other Copepoda and

1170 Metridinidae at higher latitudes and by Calanoida, Ostracoda and Oncaeidae at lower latitudes.

1171 Polar and temperate waters displayed lower mesozooplankton diversity but higher

1172 mesozooplankton abundances/biomass, more intense vertical particle fluxes, and stronger

1173 particle attenuation rates. On the opposite, the warmer and more oligotrophic tropical waters

1174 displayed lower diversity, lower mesozooplankton biomass/ abundance, but higher attenuation

1175 rates of mesozooplankton organisms. To better disentangle the relationships between

1176   mesozooplankton composition and the environmental conditions within the different vertical

1177   layers of the ocean, separate RDAs were then performed for each depth layer.

1178

1179
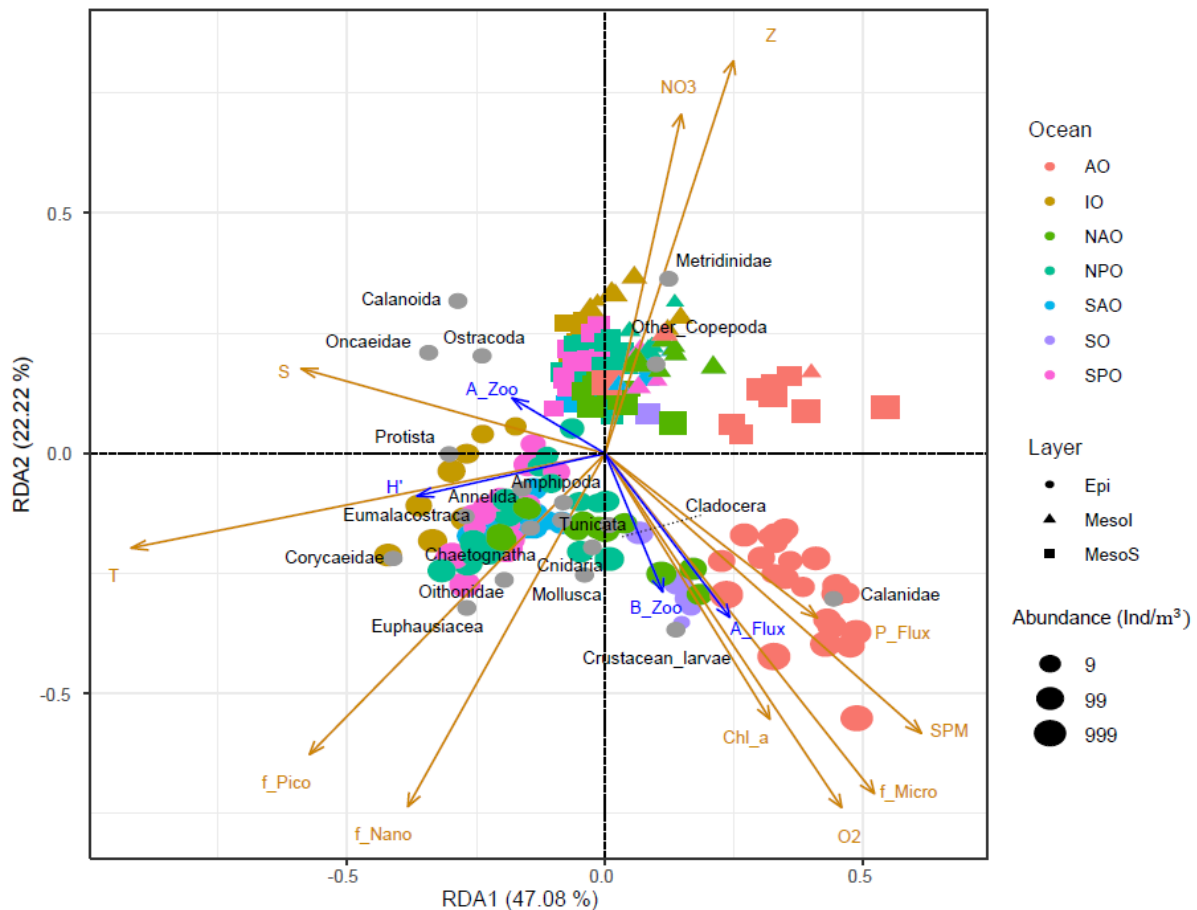
1180

1181   Figure   S2: RDA performed with all layers. Each colored dot corresponds to a sample, i.e., one net at one
1182   depth at one station. The orange arrows mark the projection of the environmental variables in RDA space:
1183   f_pico, f_nano and f_micro correspond to the relative contribution (%) of pico-, nano- and micro-phytoplankton
1184   to total phytoplankton biomass, median value of (O2 = dissolved oxygen concentration (µmol/kg), Chl_a =
1185   Chlorophyll a concentration (mg/m3), SPM = suspended particles matter (m/sr), T = temperature (°C), Sal =
1186   salinity, NO3 = nitrate concentration (mol/L), Z = depth (m)) and P_Flux= particulate flux ($mg.m^{-2}.d^{-1}$)).
1187   Grey dots mark the projection of the zooplankton groups abundance ($ind.m^{-3}$). Colors correspond to the ocean
1188   basin where the samples were taken: AO = Arctic Ocean, IO = Indian Ocean, NAO = North Atlantic Ocean,
1189   NPO = North Pacific Ocean, SAO = South Atlantic Ocean, SO = Southern Ocean, SPO = South Pacific Ocean.
1190   Shapes illustrate the vertical layers where the samples were taken: Epi = epipelagic, MesoS = upper mesopelagic
1191   and MesoI = lower mesopelagic.

1192
1193

1194

1195 Table S1: List of nets that were removed from the RDA analysis. AO=Arctic Ocean, IO=Indian Ocean,

1196 NAO=North Atlantic Ocean, NPO=North Pacific Ocean, SAO=South Atlantic Ocean, SO=Southern

1197 Ocean or Austral Ocean, SPO=South Pacific Ocean.

Ocean Bassin	Nets
IO	36_4,38_4, 39_2, 42_3
AO	163_2, 163_3, 206_2
NAO	142_4,142_4n,143_3,143_3n,147_3,147_4,150_1,150_4,151_2,151_4,152_2,152_3,155_2,158_2
NPO	131_2, 132_2,133_3,135_2,137_3,137_3n
SAO	131_2, 132_2,133_3,135_2,137_3,137_3n
SO	84_1, 85_1, 85_2
SP0	98_2, 98_3, 102_1, 106_2, 106_4,109_1,110_1,110_1n,111_1,111_1n,122_1,122_1n,125_1,125_3,127_2,127_2n

1198

1199

1200

1201 Table S2: Wilcoxon test for day and night for each taxon at level of 5% (bold values mean significant

1202 test)

Species	Wilcoxon p-value (abundance)		Wilcoxon p-value (biomass)	
	Epipelagic	Upper Mesopelgic	Epipelagic	Upper Mesopelgic
Protista	0.50	0.13	0.8	0.06
Annelida	0.66	0.82	0.62	0.57
Chaetognatha	1	0.20	0.58	0.32
Tunicata	0.26	0.078	0.06	0.19
Cnidaria	0.90	**0.037**	0.58	**0.009**
Mollusca	0.95	0.123	0.26	0.96
Eumalacostraca	0.39	0.62	**0.049**	0.49
Euphausiacea	0.21	**0.0098**	**0.0001**	0.63
Amphipoda	0.07	0.91	0.39	0.83
Ostracoda	0.32	0.96	**0.049**	1
Crustacean_larvae	**0.01**	0.81	0.23	0.81
Other_Copepoda	0.76	0.46	0.95	0.41
Calanoida	0.10	0.24	0.11	0.32
Oithonidae	0.19	1	0.24	0.84
Corycaeidae	**0.01**	1	**0.016**	0.76
Oncaeidae	0.66	0.41	0.8	0.51
Metridinidae	**0.0001**	**0.018**	**0.0001**	**0.006**
Calanidae	0.29	0.12	0.07	1

1203
1204
1205
1206
1207
1208

1209